Efficient Spatial Index for 3D Object Retrieval (Technical Report)

ABSTRACT

Due to the growth of the 3D technology, digital 3D models represented in the form of point clouds have attracted a lot of attention from both industry and academic. In this paper, due to a variety of different applications, we study a fundamental problem called the *3D object retrieval*, which is to find a set of 3D point clouds stored in a database which are similar to a given query 3D point cloud. In this paper, we propose a framework called C_2O to find the answer efficiently with the help of an index built on the database. In most of our experiments, C_2O performs up to 2 orders of magnitude faster than all adapted algorithms in the literature.

1 INTRODUCTION

Recently, digital 3D models represented in the form of point clouds have attracted a lot of attention from both industry and academic due to the increasing popularity of low-cost 3D depth sensors and LiDAR sensors [20, 41]. In industry, both hardware and software are now using 3D point clouds. For hardware, some recent mobile devices like iPhone 13 Pro, iPhone 12 Pro, iPad Pro and Samsung's Galaxy S22 use LiDAR sensors or other technology to obtain 3D point clouds easily. For software, Google is now using 3D point clouds in their products. One example is that some of the recent 3D street view images in Google Maps were generated from 3D point clouds taken by LiDAR sensors starting from 2017. Another example is that Google mobile apps started to include a library about 3D point clouds (called "PointCloud") in their software development kit "ARCore" for the augmented reality (AR) application. Due to the recent LiDAR technology usage in both software and hardware, there are different industrial domains using 3D point clouds. One example is the civil engineering domain which is using 3D point clouds in their building information models (BIM) for design, construction and maintenance. Another example is the property agency domain which is currently using 3D point clouds for visualizing a 3D first-person view of a property in the virtual reality(VR)-like application. In academic, there are a lot of research projects on point clouds. Some examples are 3D reconstruction [11], indoor robotics [33], autonomous driving [18] and VR/AR [37]. In Figure 1, there are five 3D objects each of which is represented by a *point cloud* where a point cloud is defined to be a set of points in a 3D space.
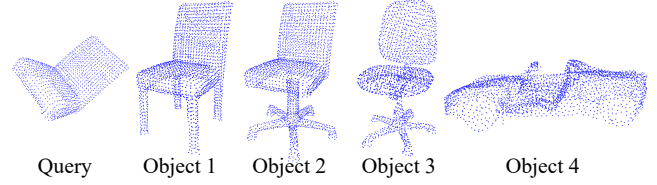
Figure 1: A Motivating Example

In most (if not all) of the applications on 3D point clouds, *3D object retrieval* is one fundamental problem. Specifically, we are given a set $\mathcal{P}$ of a number of point clouds (each representing a 3D object). Given a query point cloud Q and a user parameter δ where δ is a non-negative real number, we want to find a set of point clouds in $\mathcal{P}$ such that for each point cloud P in the set, Q is *similar* to a portion of P (and more formally, the *distance* between Q and a portion of P is at most δ). If δ is set to 0, it is an exact match between Q and a portion of a point cloud P. If δ is set to a value larger than 0, it is a similarity search problem between Q and a portion of a point cloud P. Consider Figure 1 where $\mathcal{P}$ contains Objects 1–4. Suppose that our query point cloud is shown in the figure and δ is set to a positive value near to 0. Our 3D object retrieval returns Object 1 and Object 2 in the answer (not Object 3) since both Object 1 and Object 2 contain the back rest part which is similar to the query but Object 3 does not.

There are a lot of applications about 3D object retrieval. (1) *3D Object Database Search:* In BIM, due to the growth of 3D printing in the building construction industry, various construction companies producing building components provide a database $\mathcal{P}$ containing all 3D models each representing a building component for other constructor companies to search for a particular 3D model Q, which becomes more common nowadays. In machine construction, similarly, the technology of 3D printing boosts the growth of the 3D object database storing all machine components. (2) *Unmanned Vehicle Localization:* When a 3D indoor scene is constructed in the form of 3D point cloud (which can be regarded as a database point cloud in $\mathcal{P}$), an unmanned vehicle could determine its location by using its LiDAR sensors to obtain a point cloud as a query point cloud Q which is used to find which portion of the whole 3D indoor scene point cloud. This becomes much more important in either indoor or a territory outside the Earth (e.g., Moon and Mars) when GPS signals are inaccurate or unavailable. (3) *Scientific Database Search:* In a scientific database $\mathcal{P}$ like a celestial database containing all stars in the galaxy, scientists would like to find a particular star pattern Q in the space in the database. They are also interested in finding a list of regions in the galaxy which have star patterns similar to a given star pattern.

To the best of our knowledge, there are two branches of existing studies in the literature which are closely related to our problem. The first branch is called *registration* [2, 9, 15, 16, 22, 32] which is different from our problem. There are two types of registration, namely *full registration* [2, 9, 22, 32] and *partial registration* [15, 16]. In full registration, we are given two point clouds, namely P_1 and

P_2, where the total number of points in P_1 is roughly equal to the total number of points in P_2. The problem of full registration is to determine whether P_1 could be translated or rotated such that the *whole* resulting point cloud is roughly equal to P_2. If yes, it will return the resulting point cloud (from P_1). Partial registration is similar to full registration but partial registration is to determine whether P_1 could be translated or rotated such that a *portion* of the resulting point cloud is roughly equal to a *portion* of P_2. However, existing studies about partial registration require that this portion should be large (e.g., more than 60%). It is worth mentioning that the registration problem (either full registration or partial registration) is different from our 3D object retrieval problem. Firstly, it only considers "mapping" *two* given 3D point clouds but we consider how to "search" for a given query point cloud in a database involving *many* 3D point clouds such that we can "map" the query point cloud with *portions* of some 3D point clouds. Secondly, partial registration considers "mapping" two given 3D point clouds with *large* portions but we consider "mapping" two 3D point clouds (one from the query 3D point cloud and the other from the database) in any arbitrary portion (which could be large or small).

The second branch is called *similarity search* (or called *shape matching*) [6, 21, 36, 40], which is to find a set of *different* portions of a given database point cloud representing a 3D scene such that each portion "looks" similar to a query object Q (e.g., chair) represented in the form of a point cloud. Specifically, each portion of a given database point cloud is encoded as an *embedding vector* by a machine learning model M and the query object Q is also encoded as an embedding vector by the same model M. These studies about similarity search are to return a set of portions whose embedding vectors have their Euclidean distance from the query embedding vector at most a given threshold value. However, since this existing problem adopts the concept of "embedding vectors" derived from 3D point clouds, the 3D point clouds returned in the output may not really be a real chair, and thus, the accuracy is not high. For example, when the query object is a chair (as shown in Figure 1), a car (as shown in Object 4 of Figure 1) is unfortunately returned by [36] as an output in our experiment. It is worth mentioning that there are some recent studies [36, 40] in this branch with problem named "object retrieval", which actually refers to the same problem as similarity search. Hence, their "object retrieval" problem is still different from our "object retrieval" problem definition and has the same inaccuracy issue. Moreover, [36, 40] do not consider rotation/translation and thus give incorrect results easily.

Unfortunately, none of adapted and existing algorithms could solve our 3D object retrieval problem well. Firstly, although no existing algorithms, originally designed for registration, directly solve the 3D object retrieval problem, we adapt these existing algorithms, namely Super4PCS [23] and GoICP [39], for our problem. All of these adapted algorithms suffer from one of the following problems. The first problem is low efficiency, particularly when the database size is large. The second problem is a very bulky index size (for those adapted algorithms using indices). Secondly, existing algorithms originally designed for similarity search, namely PointNetVLAD [36] and PCAN [40], are not accurate as described previously.

Motivated by this, we propose a novel and concise representation called *donut* to denote some important "features" of a 3D point cloud so that whenever we want to compare two point clouds, instead of comparing the coordinates of all the points in one point cloud with the coordinates of all the points in another point cloud, we just need to compare the donut representation of one point cloud with the donut representation of another point cloud. Since the donut representation of a point cloud is concise, it is easier to do a comparison. Specifically, the donut representation has the following advantages: *translation-invariant* and *rotation-invariant*. When a point cloud is compared with another point cloud, since these 2 point clouds are in 2 different spaces, we have to perform a translation operation and a rotation operation (which are very time-consuming). In Figure 1, the point cloud indicated by "Query" has to perform these operations so that it can be compared with each of the 4 database point clouds in the same space. The donut representation of a point cloud is said to be *translation-invariant* (*rotation-invariant*) if no matter whether we perform a translation (rotation) operation on the point cloud, the donut representation does not change. It is important that the donut representation is translation-invariant and rotation-invariant because it could avoid the time-consuming operations of translation and rotation.

When both the query point cloud and all database point clouds are encoded in the form of the donut representation, it is more efficient to find a list of database point clouds which are similar to the query point cloud.

In this paper, we propose an algorithm called C_2O which involves 2 phases, namely the preprocessing phase and the query phase. In the preprocessing phase, C_2O first builds an index on all database point clouds based on the donut representation. In the query phase, given a query point cloud Q, C_2O finds the set of point clouds in the database effectively with the help of the index.

Our contributions are as follows. Firstly, we propose a novel and concise representation called donut to effectively capture the important features of 3D point clouds so that retrieving similar 3D objects is very effective and efficient due to its translation-invariant property and its rotation-invariant property. Secondly, based on the donut representation, we propose an algorithm called C_2O to find a set of similar 3D objects efficiently. Thirdly, we conducted comprehensive experiments to show that our proposed algorithm C_2O is very effective and efficient. In particular, our proposed algorithm is 1-3 orders of magnitude faster than the adapted algorithms. We scale the database size up to 100 million points, a large data volume that has been applied in various real-world applications (e.g. localization [16], object recognition [19], and 3D reconstruction [27]), and we outperform all adapted algorithms since our proposed algorithm took less than 10 seconds for retrieving 3D objects but all adapted algorithms took more than 1000 seconds, which is not acceptable in real-life applications. Besides, the f-measure of our proposed algorithm is 100% but the f-measure of the existing algorithms originally designed for similarity search is around or less than 15%, which is not acceptable too.

In the rest of this paper, we give the formal definition of our 3D object retrieval in Section 2. In Section 3, we first describe our framework C_2O. Then, we present the detail of our algorithm C_2O in Section 4. In Section 5, we introduce the relevancy of existing problems and existing algorithms. In Section 6, we present our experimental results. Finally, we conclude our paper in Section 7.

2 PROBLEM DEFINITION

Consider a 3-dimensional space. A *point cloud* is defined to be a set of 3-dimensional points where each point is represented in a three-dimensional xyz coordinate. The size of a point cloud is defined to be the total number of points in this point cloud. For example, in Figure 1, all the points in "Query" form a point cloud and all the points in Object 1 form another point cloud. We are given a database $\mathcal{P}$ which contains $|\mathcal{P}|$ point clouds. Each point cloud in $\mathcal{P}$ is associated with an ID. In the application of 3D object database search, each point cloud in the database denotes a 3D object. In the application of unmanned vehicle localization, each point cloud in the database denotes a 3D scene. We define the size of a database, denoted by n, to be the sum of the sizes of all 3D point clouds in the database. Let us create a toy example as shown in Figure 2 to show our concept more easily where we have one query point cloud and we have the database $\mathcal{P}$ containing many objects but we just show Object 1 in $\mathcal{P}$ in the figure. Here, we illustrate the example in a two-dimensional space (for the ease of illustration) but the same illustration can be applied to a three-dimensional space.

When we compare two point clouds in two different coordinate systems, we have to perform a *rigid transformation* on one point cloud so that the transformed point cloud is in a consistent coordinate system with the other point cloud for comparison. A rigid transformation Θ on a point cloud is formed by a rotation operation and a translation operation such that the geometric structure of the point cloud is preserved. In geometry, a rotation operation is denoted by a 3D rotation 3×3 matrix R and a translation is denoted by a translation 3-dimensional vector t. A rigid transformation Θ is represented by a 2-tuple (R, t). Given a point p (represented in a 3-dimensional vector) and a transformation $\Theta = (R, t)$, the *transformed point* of p wrt Θ, denoted by $T_\Theta(p)$, is defined as follows: $T_\Theta(p) = Rp + t$. In other words, point p is rotated with the rotation matrix R and is translated with the translation vector t. Given a point cloud P, we define the *transformed point cloud* of P wrt Θ, denoted by $T_\Theta(P)$, to be $\{T_\Theta(p) \mid p \in P\}$. Figure 3(a) shows the query point cloud from Figure 2 rotated with 45° clockwise and Figure 3(b) shows the query point cloud from Figure 2 rotated with 135° clockwise.

In our problem, we need to compare a query point cloud with a database point cloud. We just need to do a rigid transformation on one point cloud, which is chosen as the query point cloud in this paper. Figure 4 shows the rotated query point cloud in Figure 3(a) in the coordinate system of Object 1 which undergoes a translation operation, which is indicated in a dashed rectangle R_1. Similarly, Figure 4 also shows the rotated query point cloud in Figure 3(b) in the coordinate system of Object 1 which undergoes a translation operation, which is indicated in a dashed rectangle R_2.

Let us consider how we define the distance between two point clouds in the same coordinate system for easier illustration. After that, we will consider the case when the two point clouds are in different coordinate systems. Consider two point clouds in the same coordinate system, namely Q and P. For each point q in Q, we define the *correspondence point* of q on P, denoted by $corr(q, P)$, to be the closest point of q in P (which is a common definition in the literature [4]). We denote the Euclidean distance between point q and point p by $\|q, p\|$. The distance between Q and P in the same coordinate system, denoted by $dist_{same}(Q, P)$, is defined as follows

based on the concept of the L_2-norm.

$$dist_{same}(Q, P) = \left[\frac{1}{|Q|} \sum_{q \in Q} \|q, corr(q, P)\|^2 \right]^{\frac{1}{2}} \quad (1)$$

Consider back Figure 4. We know that the rotated query point cloud Q' in R_1 is in the same coordinate system of Object 1. Suppose that P is the point cloud denoting Object 1. In this figure, we know that the correspondence point of q'_1 on P is p_1 (i.e., $corr(q'_1, P) = p_1$) and the correspondence point of q'_2 on P is p_4 (i.e., $corr(q'_2, P) = p_4$). After we find the correspondence point of each point in the rotated query point cloud Q', we can compute the distance between Q' and P (i.e., $dist_{same}(Q', P)$). Note that since *visually*, each query point in Q' is very close to a point in P, the distance between Q' and P is very small (e.g., near to 0). It is easy to have a similar conclusion for the rotated query point cloud Q'' in R_2. Note that since q''_5 is a little bit far away from its closest point in P (i.e., p_7) (compared with other points in Q''), we derive that $dist_{same}(Q'', P) > dist_{same}(Q', P)$.

However, as mentioned before, typically, two given point clouds are usually not in the same coordinate system. We have to perform a rigid transformation on one point cloud (in our case, the query point cloud). Consider two point clouds in different coordinate systems, namely Q and P. Given a transformation Θ on Q, the distance between Q and P in different coordinate systems wrt Θ, denoted by $dist_{diff}(Q, P|\Theta)$, is defined as follows.

$$dist_{diff}(Q, P|\Theta) = \left[\frac{1}{|Q|} \sum_{q' \in T_\Theta(Q)} \|q', corr(q', P)\|^2 \right]^{\frac{1}{2}} \quad (2)$$

It is the same as Equation 1 except that we include the rigid transformation Θ on Q only in the above equation.

Let Θ_o be the optimal rigid transformation in a set $\mathcal{T}$ of all possible transformations of Q such that Equation 2 is minimized. That is, $\Theta_o = \arg\min_{\Theta \in \mathcal{T}} \left[\frac{1}{|Q|} \sum_{q' \in T_\Theta(Q)} \|q', corr(q', P)\|^2 \right]^{\frac{1}{2}}$. We overload symbol $dist_{diff}(\cdot, \cdot)$ and define the distance between Q and P in different coordinate systems, denoted by $dist_{diff}(Q, P)$, to be the following.

$$dist_{diff}(Q, P) = \left[\frac{1}{|Q|} \sum_{q' \in T_{\Theta_o}(Q)} \|q', corr(q', P)\|^2 \right]^{\frac{1}{2}} \quad (3)$$

In the following, for the sake of simplicity, when we write $dist(Q, P)$, we mean $dist_{diff}(Q, P)$.

Definition 2.1 (3D Object Retrieval). Given a query point cloud Q and a user parameter δ where δ is a non-negative real number, we want to find a set of point clouds in $\mathcal{P}$ such that for each point cloud P in the set, $dist(Q, P) \le \delta$.

3 FRAMEWORK C_2O

In our 3D object retrieval problem, we have to check whether a given query point cloud Q and a given point cloud P in the database $\mathcal{P}$ have $dist(Q, P) \le \delta$. We propose our framework called C_2O which involves the following 3 major steps to complete this goal.

- **Step 1 (Coarse Transformation):** We first perform a *rough* or *coarse* transformation Θ on Q based on *some* "representative" points of Q so that the transformed point cloud of Q and the point cloud P are in the same coordinate system. The reason why there is a coarse transformation is that finding an *optimal* transformation is costly. The time complexity of finding an optimal transformation is $O(8^l)$ [39], where l is a data-dependent parameter (and is about 30 on average in our experiment). In a typical
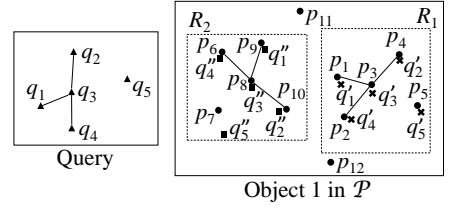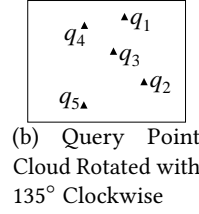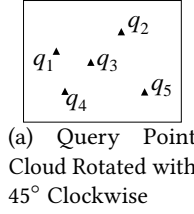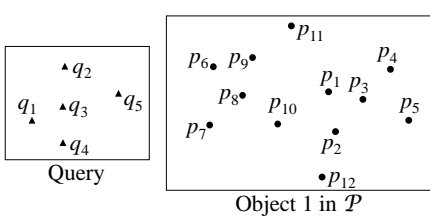
Figure 2: Examples of Database and Query Point Clouds

Figure 3: Examples of Rotated Query Point Clouds

Figure 4: Examples of Transformation and Retrieval

experimental setting (e.g., with the database size 1M and the query size 100), finding an optimal transformation from *scratch* takes more than 1000 seconds but finding a rough transformation from some points in Q takes about 0.5 second only.

- **Step 2 (Complete Transformation):** We then perform a *complete* transformation Θ_o on Q based on *all* points of Q according to the initial coarse transformation Θ so that the transformation on Q is optimal. Note that with the help of the initial transformation Θ, finding the optimal transformation is much faster. In our experiment (e.g., a typical setting described above), it takes 0.9 second only.

- **Step 3 (Object Retrieval):** After we obtain the optimal transformation Θ_o on Q, we can compute $dist_{diff}(Q, P|\Theta_o)(= dist(Q, P))$ easily and check whether $dist(Q, P) \leq \delta$. If yes, P will be in the answer of our 3D object retrieval.

The most challenging step in framework C_2O is coarse transformation, because finding a "close-to-optimal" transformation based on some "representative" points of Q could be costly (though much cheaper than finding the optimal one) since searching "representative" points blindly may not help to improve the efficiency.

One may ask the following question. How could we obtain some "representative" points of Q in Step 1 so that we could execute coarse transformation efficiently? In this paper, we propose a novel and concise representation of a given point cloud called the *donut* representation. Specifically, each point in a given point cloud can be encoded in a representation called the *relative-distance representation* which is represented in the form of a 6-dimensional tuple where each dimension in this tuple is a real number. For each point $p_{(1)}$ in P, we find 3 other points in P in a particular order, say $p_{(2)}$, $p_{(3)}$ and $p_{(4)}$, based on the principle of the *regular tetrahedron* (to be elaborated in detail later) and compute the relative-distance representation according to the pairwise distances among these 4 points. The relative-distance representation of point $p_{(1)}$ wrt the other 3 points (i.e., $p_{(2)}$, $p_{(3)}$ and $p_{(4)}$), denoted by $rd(p_{(1)}|p_{(2)}, p_{(3)}, p_{(4)})$, is defined as follows. That is, $rd(p_{(1)}|p_{(2)}, p_{(3)}, p_{(4)}) =$

$$(\|p_{(1)}, p_{(2)}\|, \|p_{(1)}, p_{(3)}\|, \|p_{(1)}, p_{(4)}\|,$$
$$\|p_{(2)}, p_{(3)}\|, \|p_{(2)}, p_{(4)}\|, \|p_{(3)}, p_{(4)}\|) \tag{4}$$

We define the *first, second, third, fourth owners* of this representation to be $p_{(1)}$, $p_{(2)}$, $p_{(3)}$ and $p_{(4)}$, respectively. The donut representation of a point cloud is defined to be a collection of relative-distance representations of all points in this point cloud. More importantly, due to the property that the relative-distance representation considers only *relative* distance computation, as described in Section 1, this donut representation (or the relative-distance representation) satisfies the translation-invariant property and the rotation-invariant

property. These properties ensure that given a set S of 4 points, even if we obtain a set S' of 4 points which are the 4 resulting points of S rotated with any angle and translated with any value where each of these points may deviate from its original coordinate with some distance, the relative-distance representation generated based on S is "close" to the one generated based on S'.

After we have the concept of "relative-distance representation", one may give the following naive implementation of framework C_2O when we consider a query point cloud Q and *one* data point cloud P. In Step 1, given a query point cloud Q, we randomly pick a point q in Q to generate its *relative-distance representation* R_q. Based on the representation R_q, for each point p in a data point cloud P, we check with the relative-distance representation of p, say R_p. If R_q and R_p are close, we can find the (coarse) transformation Θ according to the 4 selected points in Q and the 4 selected points in P. In Step 2, according to the (coarse) transformation Θ, we derive a (complete) transformation Θ_o according to all points in Q and all points in P using the state-of-the-art algorithm called Go-ICP [39] which is guaranteed to return the optimal transformation. In Step 3, we check whether $dist_{diff}(Q, P|\Theta_o) \leq \delta$. If the answer is yes, we include P in the output.

Since typically, there are more than one point cloud in the database, the naive implementation has to process one point cloud by one point cloud in the database and compare each point cloud in the database with the query point cloud, which is very time-consuming.

In this paper, we propose an index-based approach which involves 2 phases, namely the preprocessing phase and the query phase. In the preprocessing phase, we build an index on all point clouds in $\mathcal{P}$ according to the concept of "relative-distance representation". In the query phase, given a query point cloud, we just randomly find a point in Q and use its relative-distance representation to find the similar representations stored in the index efficiently.

4 ALGORITHM C_2O

We first give the details of the donut representation (containing a number of relative-distance representations of points in a point cloud) in Section 4.1. Then, we describe how the relative-distance representation of a point in a *data* point cloud could be matched with that of a point in a *query* point cloud in Section 4.2. Finally, we give the details of our proposed algorithm C_2O in Section 4.3.

4.1 Donut Representation

In this section, we give the details of the donut representation. The major principle of this donut representation is to generate a 6-dimensional tuple (called the *relative-distance representation*) according to the concept of "regular tetrahedron". There are two
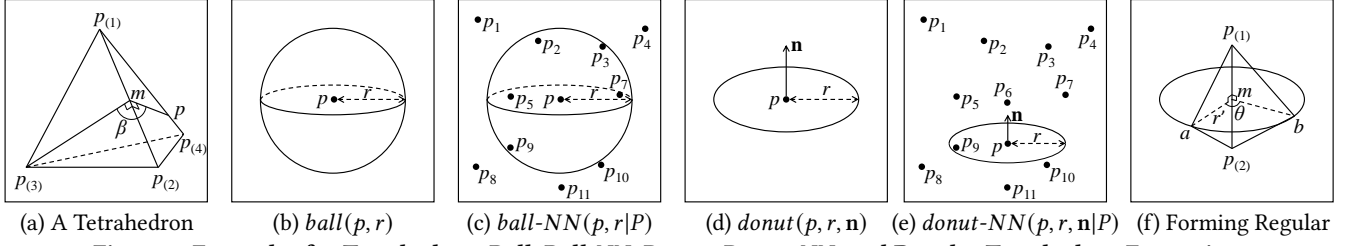
(a) A Tetrahedron   (b) $ball(p, r)$ (c) $ball\text{-}NN(p, r|P)$ (d) $donut(p, r, \mathbf{n})$ (e) $donut\text{-}NN(p, r, \mathbf{n}|P)$ (f) Forming Regular

Figure 5: Examples for Tetrahedron, Ball, Ball-NN, Donut, Donut-NN, and Regular Tetrahedron Formation

reasons why we use the concept of "regular tetrahedron". The first reason is due to the usage of tetrahedron involving 4 points. In the literature [2, 7], it is found that using 4 points to represent some local structures of the 3D point cloud could give more differentiating power for pruning (compared with the one using 3 points which is another branch in the literature). The second reason is due to the usage of "regularity". It is found in [24] that more regular shapes could have more differentiating power. It is worth mentioning that our proposed concept of "regular tetrahedron" is different from existing representations in the literature. Firstly, existing representations of 4 points are separated into two point-pairs (each connected with a line segment) and a connector connecting the two line segments [2, 25], which leads to the costly two-step pruning that is first based on the two point-pairs and then based on the connector. We consider a "holistic" shape of 4 points (i.e., a tetrahedron), and thus our pruning can be efficiently done in one step. Secondly, the 4 points in our representation are *ordered* but the 4 points in the existing representations [2, 24, 25] are *unordered*, which means that we do not need to enumerate all possible 4-point combinations, required by the existing representations, for searching the corresponding 4 points in a database object given a 4-point representation in a query object, and thus our representation is much more efficient during the search.

Given 4 points in a 3D space, namely $p_{(1)}, p_{(2)}, p_{(3)}$ and $p_{(4)}$, a *tetrahedron* is defined to be a polyhedron composed of four triangular faces, six straight edges and four vertex corners where $p_{(1)}, p_{(2)}, p_{(3)}$ and $p_{(4)}$ form the 4 corners. We can also say that this tetrahedron is represented by these 4 points. One example of a tetrahedron can be found in Figure 5(a). Note that m is a point on edge $p_{(1)}p_{(2)}$. Suppose that line $p_{(3)}m$ is perpendicular to line $p_{(1)}p_{(2)}$, and line pm is perpendicular to line $p_{(1)}p_{(2)}$. Clearly, $\beta = \angle p_{(3)}mp$ is the dihedral angle between face $p_{(1)}p_{(2)}p_{(3)}$ and face $p_{(1)}p_{(2)}p_{(4)}$. The *size* of a tetrahedron is defined to be the maximum length of an edge in the tetrahedron. A tetrahedron is said to be *regular* if the lengths of edges are equal. Given a non-negative real number r, a tetrahedron is said to be an *r-sized regular tetrahedron* if the size of this tetrahedron is r and this tetrahedron is regular. Besides, the dihedral angle between any two adjacent faces in a regular tetrahedron is equal to $\arccos 1/3$ radian. It is easy to verify that in Figure 5(a), if the tetrahedron is regular, and m is the mid-point between $p_{(1)}$ and $p_{(2)}$, then the length of line $p_{(3)}m$ is equal to $\frac{\sqrt{3}}{2}\|p_{(1)}, p_{(2)}\|$. In this case, p is exactly $p_{(4)}$. Then, the length of line $p_{(4)}m$ (or line pm) is equal to $\frac{\sqrt{3}}{2}\|p_{(1)}, p_{(2)}\|$ too.

We are now ready to describe the relative-distance representation. Specifically, given a data point cloud P, for each point $p_{(1)}$ in P, we construct its relative-distance representation as follows.

- **Step 1 (Forming Tetrahedron):** We find 3 other points in P from $p_{(1)}$ in a *particular* order, namely $p_{(2)}, p_{(3)}$ and $p_{(4)}$, such that the 4 points found can form a tetrahedron (where the 4 vertices of this tetrahedron are these 4 points) and this tetrahedron is as close as an R-sized regular tetrahedron where R is a non-negative real number which is roughly equal to a user parameter r, a non-negative real number.
- **Step 2 (Constructing Relative-Distance Representation):** According to these 4 points found, we construct the relative-distance representation (which is a 6-dimensional tuple) based on all the pairwise distances among these 4 points.

Step 2 is straightforward. Next, we give the details of Step 1. We are given a point $p_{(1)}$ in a point cloud P. In the following, we describe how we find the 3 other points in P from $p_{(1)}$ in a particular order. Before that, we first define the concept of "ball" and the concept of "donut".

Given a 3D point p and a non-negative real number r, the *r-sized ball of p*, denoted by $ball(p, r)$, is defined to be the surface of a sphere centered at p with radius equal to r. Given a 3D point p and a non-negative real number r, the *nearest neighbor of the r-sized ball of p in P*, denoted by $ball\text{-}NN(p, r|P)$, is defined to be the point in P which is the nearest to a point in the r-sized ball of p (i.e., $ball(p, r)$) and has its distance to p at least r. Figure 5(b) shows an example of $ball(p, r)$ and Figure 5(c) shows that point p_{10} in P is $ball\text{-}NN(p, r|P)$.

Next, we define the concept of "donut". Given a 3D point p, a non-negative real number r and a 3D vector $\mathbf{n}$, the *r-sized donut of p with its normal $\mathbf{n}$*, denoted by $donut(p, r, \mathbf{n})$, is defined to be the boundary of a circle centered at p with radius equal to r which is on the plane with its (surface) normal equal to $\mathbf{n}$. Given a 3D point p, a non-negative real number r and a 3D vector $\mathbf{n}$, the *nearest neighbor of the r-sized donut of p with its normal $\mathbf{n}$ in P*, denoted by $donut\text{-}NN(p, r, \mathbf{n}|P)$, is defined to be the point in P which is nearest to a point in the r-sized donut of p with its normal $\mathbf{n}$ (i.e., $donut(p, r, \mathbf{n})$). Figure 5(d) shows an example of $donut(p, r, \mathbf{n})$ and Figure 5(e) shows that point p_9 in P is $donut\text{-}NN(p, r, \mathbf{n}|P)$.

We defined the concept of "ball" and the concept of "donut". Based on these 2 concepts, we can give our principle of constructing a regular tetrahedron involving 4 points. In order to construct a tetrahedron T involving 4 points from P (i.e., $p_{(1)}, p_{(2)}, p_{(3)}$ and $p_{(4)}$) (which is not necessarily regular in most cases), we construct a *virtual* regular tetrahedron. In this virtual regular tetrahedron involving 4 points in a particular order, the first 2 points are points in P (which are assigned to $p_{(1)}$ and $p_{(2)}$, respectively), and the latter 2 points are *virtual* points, namely a and b (which may not be in P). The size of this regular tetrahedron (denoted by R) is determined in the following process but its value is near to a user parameter r.

In the final tetrahedron T involving 4 points (which come from P), the first 2 points are exactly $p_{(1)}$ and $p_{(2)}$, and the final 2 points, namely $p_{(3)}$ and $p_{(4)}$, are "close" to points a and b, respectively.

The steps of finding these 4 points in P (together with points a and b) are described as follows. Firstly, we start with a point in P, say $p_{(1)}$. Then, according to a user parameter r (which is a non-negative real number), we find another point in P, say $p_{(2)}$, which is the nearest to $p_{(1)}$ with distance from $p_{(1)}$ at least r (i.e., $ball\text{-}NN(p_{(1)}, r|P)$). Then, according to $p_{(1)}$ and $p_{(2)}$, we form a virtual regular tetrahedron as follows where the size of this tetrahedron (i.e., R) is equal to $\|p_{(1)}, p_{(2)}\|$ (typically, R is close to r in practice and in our experiments, R is at most 1.1 times r). We construct a *locus* of a point denoting D such that this point has its distance to $p_{(1)}$ and its distance to $p_{(2)}$ both equal to $\|p_{(1)}, p_{(2)}\|$. Let m be the mid-point between $p_{(1)}$ and $p_{(2)}$, and $\mathbf{n}$ be a vector from $p_{(2)}$ to $p_{(1)}$. It is easy to verify that this locus is equal to $donut(m, r', \mathbf{n})$, where r' is defined to be $\frac{\sqrt{3}}{2}\|p_{(1)}, p_{(2)}\|$. This is because for each point in this locus, its distance to $p_{(1)}$ and its distance to $p_{(2)}$ are both equal to $\|p_{(1)}, p_{(2)}\|$. Since the shape of the locus is similar to "donut", this is the reason why we call this as the donut representation. According to this locus, we find the point in P nearest to this locus (i.e., $donut\text{-}NN(m, r', \mathbf{n}|P)$), which is assigned to $p_{(3)}$. Then, the point on the locus which is nearest to $p_{(3)}$ can be determined and is assigned to a. Then, according to $p_{(1)}, p_{(2)}$ and a, we can virtually construct a regular tetrahedron with 4 vertices. The first 3 vertices of the regular tetrahedron are $p_{(1)}, p_{(2)}$ and a. It is easy to know that the last vertex of this tetrahedron (i.e., b) can be found on two possible positions along the locus. For a more deterministic formation of the regular tetrahedron, we adopt the strategy to find the position (among these 2 positions) as the position of point b which is the position closest to a in the anti-clockwise direction from a on the locus (in the view point from $p_{(1)}$ to $p_{(2)}$). Figure 5(f) illustrates point b in the regular tetrahedron. Then, we find the point in P nearest to b, which is assigned to $p_{(4)}$. Thus, finally, we obtain all 4 points in P (i.e., $p_{(1)}, p_{(2)}, p_{(3)}$ and $p_{(4)}$).

Consider our example as shown in Figure 6(a). Suppose that we would like to form a tetrahedron starting from point p_6. Note that $p_{(1)} = p_6$. Firstly, we assign p_{11} as $p_{(2)}$ (since p_{11} is $ball\text{-}NN(p_6, r|P)$). Secondly, in the figure, m is the mid-point between p_6 and p_{11}. We denote $\mathbf{n}$ as the direction vector from p_{11} to p_6. Let $r' = \frac{\sqrt{3}}{2}\|p_{(1)}, p_{(2)}\|$. We denote $donut(m, r', \mathbf{n})$ by D. $donut\text{-}NN(m, r', \mathbf{n}|P)$ is equal to p_9, which is assigned to $p_{(3)}$. Note that a is the nearest point to p_9 on this donut. Thirdly, in the figure, b is a point on the donut which is in the anti-clockwise direction from a (indicated by the blue arrow) (in the view point from p_6 to p_{11}). We find the nearest point in P to b (i.e., p_{10}) which is assigned to $p_{(4)}$.

Note that the above steps generate a tetrahedron (represented by $p_{(1)}, p_{(2)}, p_{(3)}$ and $p_{(4)}$) which is close to a regular tetrahedron (which is represented by $p_{(1)}, p_{(2)}, a$ and b).

With these 4 points (i.e., $p_{(1)}, p_{(2)}, p_{(3)}$ and $p_{(4)}$), we can construct the relative-distance representation as shown in Equation 4.

4.2 Matching Relative-Distance Representation

In this section, we describe how the relative-distance representation of a point in a *data* point cloud can be matched with that of a point
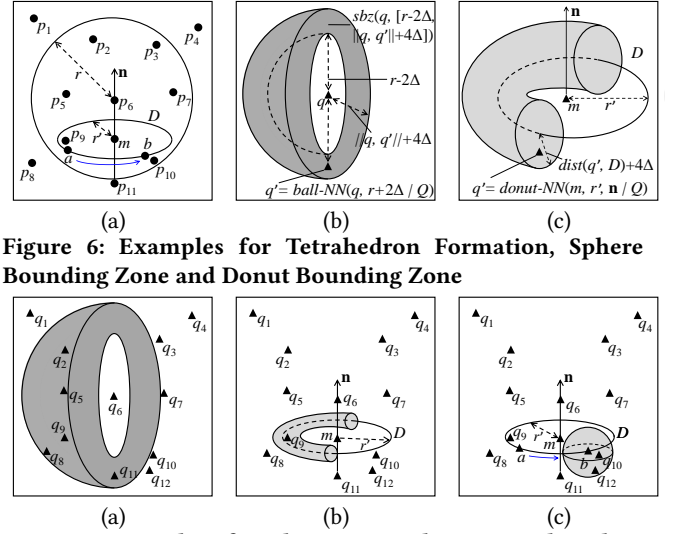

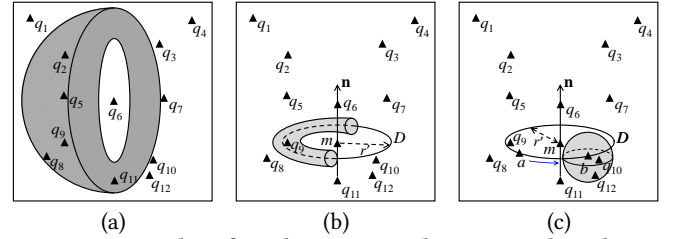**Figure 6: Examples for Tetrahedron Formation, Sphere Bounding Zone and Donut Bounding Zone**

Figure 7: Examples of Finding $S_{(2)}$, Finding $S_{(3)}$ and Finding $S_{(4)}$

in a *query* point cloud even though there is an order enforced when we find the 3 other points from a point (e.g., $p_{(1)}$).

Consider a query point cloud Q and a data point cloud P in $\mathcal{P}$. In our problem, we want to determine whether $dist(Q, P) \leq \delta$. When δ is greater than 0, this means that after an optimal transformation on Q resulting in a transformed point cloud Q', each point q' in Q' has its correspondence point p on P such that $\|q', p\|$ *could* be greater than 0. However, since δ is a fixed value, $\|q', p\|$ can be upper bounded by a fixed value too. The following lemma shows the upper bound of $\|q', p\|$ according to δ.

LEMMA 4.1. *Let Q' be the point cloud optimally transformed from Q (wrt P). If $dist(Q, P) \leq \delta$, then for each point q' in Q' and its correspondence point p on P, $\|q', p\| \leq \delta|Q|^{1/2}$.*

PROOF SKETCH. Note that $\|q', p\|^2$ is at most the sum of all squared distances (which is at most $\delta^2|Q|$ by definition). The proof is done by squaring root both sides of the inequality. □

Let $\triangle = \delta|Q|^{1/2}$. Based on this lemma, we derive a property called *Distance Bound Property* stating that the distance between each (transformed) query point and its correspondence on P is bounded by $\triangle$.

Now, we are ready to describe how the relative-distance representation of a point in the query point cloud Q (generated based on 4 points in Q) can be used to "map" with the relative-distance representation of a point in the data point cloud P (generated based on 4 points in P). This involves the following steps.

- **Step (a) (Finding Query Point):** We randomly pick a point in Q, say $q_{(1)}$.
- **Step (b) (Constructing Relative-Distance Representation Candidates):** We construct a set of candidates of the relative-distance representation of $q_{(1)}$.
- **Step (c) (Finding Answers from Database):** For each candidate c in Step (b), we find a list of point clouds in $\mathcal{P}$ according to the relative-distance representations of all point clouds in $\mathcal{P}$ and the candidate c.

Step (a) is straightforward. Doing Step (b) *efficiently* is non-trivial. Consider a point cloud P in $\mathcal{P}$. Suppose that $dist(Q, P) \leq \delta$. We know that each point q in Q has its correspondence point on P (i.e., $corr(q, P)$) when we compute $dist(Q, P)$. Since each point in P finds 3 other points in P in a *particular order* (based on the principle of regular tetrahedron) and constructs its relative-distance representation, for effective mapping between Q and P based on their relative-distance representations, one method of finding 3 other points in Q from a randomly chosen point $q_{(1)}$ (from Step (a)) whose correspondence point on P is $p_{(1)}$ is described as follows. Let $p_{(2)}, p_{(3)}$ and $p_{(4)}$ be the second, third and fourth owners of the relative-distance representation of $p_{(1)}$, respectively. The method is to find an ordering of the other 3 points in Q, say $q_{(2)}, q_{(3)}$ and $q_{(4)}$, whose correspondence points on P are $p_{(2)}, p_{(3)}$ and $p_{(4)}$, respectively. In other words, the ordering of the 4 points in Q (i.e., $(q_{(1)}, q_{(2)}, q_{(3)}, q_{(4)})$) is consistent with the ordering of the 4 points in P (i.e., $(p_{(1)}, p_{(2)}, p_{(3)}, p_{(4)})$).

One naive implementation of Step (b) is to enumerate *all combinations* among all 4 points in Q (i.e., the Cartesian product of $Q \times Q \times Q \times Q$) as candidates, denoting all possible orderings of 4 points in Q, and to construct their relative-distance representations. Although one combination (denoting one ordering of 4 points in Q) is consistent with the ordering of their (correspondence) points in P, this implementation is quite expensive. In the following, we describe how to do it efficiently by finding a *small* subset of these combinations only. The major idea is to generate this small (candidate) set of these combinations based on two major principles. The first principle is to follow Distance Bound Property and the second principle is to follow how to find the 4 points in a point cloud (as described in Section 4.1). Based on these principles, many combinations could be pruned and thus, a small candidate set could be obtained. Once we obtain the candidate set in Step (b), we can do Step (c) easily by comparing each candidate in Step (b) with point clouds in $\mathcal{P}$ according to their relative-distance representations. Later, in Section 4.3, we describe how we use an index to further speed up this step.

In the following, we propose an efficient method to find a set of candidates much more *efficiently* for Step (b). Firstly, we start from point $q_{(1)}$ (obtained from Step (a)). Secondly, based on the two major principles, we find a set $S_{(2)}$ of candidate points in Q for point $q_{(2)}$ according to $q_{(1)}$ (Section 4.2.1). Similarly, based on the principles, we find a set $S_{(3)}$ of candidate points in Q for point $q_{(3)}$ according to $q_{(1)}$ and $q_{(2)}$ (Section 4.2.2). We do the same to find a set $S_{(4)}$ for point $q_{(4)}$ according to $q_{(1)}, q_{(2)}$ and $q_{(3)}$ (Section 4.2.3). Then, we construct a candidate set of all relative-distance representations according to $\{q_{(1)}\}$, $S_{(2)}$, $S_{(3)}$ and $S_{(4)}$ (Section 4.2.4). This candidate set corresponds to the output of Step (b). Note that $\{q_{(1)}\}$ is much smaller than Q and $S_{(i)}$ is also much smaller than Q for each $i \in [2, 4]$, and thus, this candidate set is much smaller than the Cartesian product of $Q \times Q \times Q \times Q$.

4.2.1 Finding $S_{(2)}$. In the following, we describe how to find $S_{(2)}$ according to $q_{(1)}$ first based on the two principles. Before that, we first define some concepts whose major ideas come from the two principles. Given two non-negative real numbers, namely r_1 and r_2, where $r_1 \leq r_2$, we define an *interval*, denoted by $[r_1, r_2]$, to represent all values such that each value is at least r_1 and at most r_2.

Given a 3D point p and an interval $[r_1, r_2]$ where $r_1 < r_2$, the *sphere boundary zone* of p with interval $[r_1, r_2]$, denoted by $sbz(p, [r_1, r_2])$, is defined to be the 3D space containing all 3D points such that each point in this space has its distance to p at least r_1 and at most r_2.

In Figure 6(b), the shaded region is $sbz(q, [r_1, r_2])$ where $r_1 = r - 2\triangle$, $r_2 = \|q, q'\| + 4\triangle$ and $q' = ball\text{-}NN(q, r + 2\triangle|Q)$. For better illustration, in the figure, we show $sbz(q, [r_1, r_2])$ in the "half-sphere", and the other "half-sphere" is just symmetric. Note that it is obvious $r_1 = r - 2\triangle \leq r \leq r_2 = \|q, q'\| + 4\triangle$.

Next, we present the idea of how to construct $S_{(2)}$. The idea is that we construct $S_{(2)}$ such that it must contain the desired $q_{(2)}$ having $p_{(2)}$ as its correspondence point on P. Since $p_{(2)}$ is the nearest neighbor of the r-sized ball of $p_{(1)}$ in P (and is very close to the r-sized ball of $p_{(1)}$ in most cases), based on the two major principles, it is guaranteed that our desired $q_{(2)}$ is also close to the r-sized ball of $q_{(1)}$ or the distance from our desired $q_{(2)}$ to $q_{(1)}$ is close to the distance from $p_{(2)}$ to $p_{(1)}$. With the concept of sphere bounding zone, we can find a set $S_{(2)}$ of *candidate* points in Q for $q_{(2)}$ such that each candidate point in $S_{(2)}$ is inside a sphere bounding zone that is close to the r-sized ball of $q_{(1)}$. Specifically, we first find a point q' to be the nearest neighbor of a $(r + 2\triangle)$-sized ball of $q_{(1)}$ in Q. Then, we find a set $S_{(2)}$ of *candidate* points in Q for $q_{(2)}$ inside region $sbz(q_{(1)}, [r - 2\triangle, \|q_{(1)}, q'\| + 4\triangle])$ such that $S_{(2)}$ must contain our desired $q_{(2)}$ and can be listed out. See Section B.2 for details.

Figure 7(a) shows an example of how to find $S_{(2)}$ in a query point cloud Q if we pick q_6 as $q_{(1)}$. The shaded region (which is also shown in the "half-sphere" for better illustration and the other "half-sphere" is symmetric) represents $sbz(q_6, [r - 2\triangle, \|q_6, q'\| + 4\triangle])$ where q_{11} is selected to be q' since $q_{11} = ball\text{-}NN(q_6, r + 2\triangle|Q)$. Therefore, $S_{(2)}$ is the set of all the points inside the shaded region (i.e., $S_{(2)} = \{q_2, q_8, q_9, q_{11}\}$). Note that $q_1, q_3, q_4, q_5, q_6, q_7, q_{10}$ and q_{12} in the figure are outside the shaded region.

4.2.2 Finding $S_{(3)}$. Next, we consider how to construct $S_{(3)}$ according to $q_{(1)}$ and $q_{(2)}$ based on the two principles where $q_{(2)} \in S_{(2)}$. Before that, we also define some concepts. Given a point q' and a donut D, the distance between q' and D, denoted by $dist(q', D)$, is defined to be the distance between q' and its nearest point on D. Given a donut D and an interval $[r_1, r_2]$, we define the *donut boundary zone* of D with an interval $[r_1, r_2]$, denoted by $dbz(D, [r_1, r_2])$, to be the 3D space containing all 3D points such that each point in this space has distance to donut D at least r_1 and at most r_2. In Figure 6(c), the shaded region is $dbz(D, [0, dist(q', D) + 4\triangle])$ (shown in "half-space").

Now, we give our idea of how to construct $S_{(3)}$. Suppose that we are given $q_{(1)}$ and $q_{(2)}$ (whose correspondence points on P are $p_{(1)}$ and $p_{(2)}$, respectively). Note that in Section 4.1, for the *database* point cloud P, the third owner of the relative-distance representation of $p_{(1)}$ (i.e., $p_{(3)}$) is the nearest point in P to a donut (constructed based on $p_{(1)}$ and $p_{(2)}$ in P). Thus, the desired $q_{(3)}$ with $p_{(3)}$ as its correspondence point on P is also close to a donut constructed from $q_{(1)}$ and $q_{(2)}$ in the same way. Specifically, we find the donut D to be $donut(m, r', \mathbf{n})$, where m is the mid-point between $q_{(1)}$ and $q_{(2)}$, $r' = \frac{\sqrt{3}}{2}\|q_{(1)}, q_{(2)}\|$ and $\mathbf{n}$ is the vector from $q_{(2)}$ to $q_{(1)}$. Then, we find a set $S_{(3)}$ of *candidate* points in Q for $q_{(3)}$ inside region $dbz(D, [0, dist(q', D) + 4\triangle])$, where $q' = $

$donut\text{-}NN(m, r', \mathbf{n}|Q)$, such that $S_{(3)}$ must contain our desired $q_{(3)}$ and can be listed out. See Section B.2 for details.

Consider the example shown in Figure 7(b) where we pick q_6 as $q_{(1)}$ and q_{11} as $q_{(2)}$. Accordingly, we find $D = donut(m, r', \mathbf{n})$ where m is the mid-point between q_6 and q_{11}, $r' = \frac{\sqrt{3}}{2}\|q_6, q_{11}\|$ and $\mathbf{n}$ is the vector from q_{11} to q_6. The shaded region (shown in the "half-space") represents $dbz(D, [0, dist(q', D) + 4\triangle])$ where q_9 is selected to be q' since $q_9 = donut\text{-}NN(m, r', \mathbf{n}|Q)$. Thus, $S_{(3)}$ is a set containing q_9 and q_{10} since they are inside the shaded region.

4.2.3 Finding $S_{(4)}$. We consider how to construct $S_{(4)}$ according to $q_{(1)}, q_{(2)}$ and $q_{(3)}$ based on the two principles where $q_{(2)} \in S_{(2)}$ and $q_{(3)} \in S_{(3)}$. Suppose that we are given $q_{(1)}, q_{(2)}$ and $q_{(3)}$ (whose correspondence points on P are $p_{(1)}, p_{(2)}$ and $p_{(3)}$, respectively). We still follow the steps in Section 4.1 to find point a (a point on donut D that is nearest to $q_{(3)}$) and point b (the point at the position closest to a in the anti-clockwise direction from a on D in the view point from $q_{(1)}$ to $q_{(2)}$). Since the fourth owner of the relative-distance representation of $p_{(1)}$ (i.e., $p_{(4)}$) is close to the second virtual point in the original steps in Section 4.1, we can find the desired $q_{(4)}$ with $p_{(4)}$ as its correspondence point on P to be close to b. Specifically, we find a set $S_{(4)}$ of *candidate* points in Q for $q_{(4)}$ inside region $sbz(b, [0, \|b, q''\| + 4\triangle])$, where q'' is the nearest neighbor of b in Q, See Section B.2 for details.

In the example shown in Figure 7(c), we pick q_6 as $q_{(1)}$, q_{11} as $q_{(2)}$ and q_9 as $q_{(3)}$. Point a is the nearest point of q_9 on D, and point b is a point on D which is in the anti-clockwise direction from a (indicated by the blue arrow) (in the view point from q_6 to q_{11}). We find q_{10} to be the nearest neighbor of b in Q (i.e., $q'' = q_{10}$), and thus we find $sbz(b, [0, \|b, q''\| + 4\triangle])$ shown as the shaded region in the figure. Since the shaded region also covers q_{12}, $S_{(4)}$ will finally contain both q_{10} and q_{12}.

4.2.4 Constructing Candidate Set. Now, we present how to construct the candidate set of relative-distance representations according to $\{q_{(1)}\}, S_{(2)}, S_{(3)}$ and $S_{(4)}$ (i.e., the details of Step (b)). We first initialize a variable C, to store the results of the candidates (in the form of a set of relative-distance representations), to an empty set.

- **Step (i) (Finding $S_{(2)}$):** Firstly, we find point q' to be *ball-NN*$(q_{(1)}, r + 2\triangle|Q)$. Secondly, we find set $S_{(2)}$ containing all points in Q inside $sbz(q_{(1)}, [r - 2\triangle, \|q_{(1)}, q'\| + 4\triangle])$. Thirdly, for each point $q_{(2)}$ in $S_{(2)}$, we do the following step.
  - **Step (i)(1) (Finding $S_{(3)}$):** Firstly, we find point m to be the mid-point between $q_{(1)}$ and $q_{(2)}$, we find vector $\mathbf{n}$ to be the vector from $q_{(2)}$ to $q_{(1)}$ and we find r' to be $\frac{\sqrt{3}}{2}\|q_{(1)}, q_{(2)}\|$. Secondly, we find donut D to be $donut(m, r', \mathbf{n})$. Thirdly, we find point q' to be $donut\text{-}NN(m, r', \mathbf{n}|Q)$. Fourthly, we find set $S_{(2)}$ containing all points in Q inside $dbz(D, [0, dist(q', D) + 4\triangle])$. Fifthly, for each point $q_{(3)}$ in $S_{(3)}$, we do the following step.
    - **Step (i)(1)(I) (Finding $S_{(4)}$):** Firstly, we find point a to be a point on D that is nearest to $q_{(3)}$. Secondly, we find point b to be the point at the position nearest to a in the anti-clockwise direction from a on D (in the view point from $q_{(1)}$ to $q_{(2)}$). Thirdly, we find point q'' to be the nearest neighbor of point b in Q. Fourthly, we find set $S_{(4)}$ containing all points in Q inside $sbz(b, [0 \|b, q''\| + 4\triangle])$. Fifthly, for each point $q_{(4)}$ in $S_{(4)}$, we do the following step.
      - **Step (i)(1)(I)-1 (Constructing all relative-distance representations):** Firstly, we obtain the relative-distance representation R to be $rd(q_{(1)}|q_{(2)}, q_{(3)}, q_{(4)})$ by Equation 4. Secondly, we associate R with $q_{(1)}, q_{(2)}, q_{(3)}$ and $q_{(4)}$. Thirdly, we insert R into the result set C of candidate relative-distance representations.

The following lemma shows the correctness of the above details for Step (b). Specifically, given a query point cloud Q and a database point cloud P, if $dist(Q, P) \leq \delta$, the output candidate set generated by Step (b) contains a relative-distance representation of $q_{(1)}$, which has a *correspondence* relative-distance representation of a point on P, says $p_{(1)}$.

LEMMA 4.2. *Consider a query point cloud Q and a database point cloud P. Let $q_{(1)}$ be a point in Q whose correspondence point on P is $p_{(1)}$. Let $p_{(2)}, p_{(3)}$ and $p_{(4)}$ be the second, third and fourth owners of the relative-distance representation of $p_{(1)}$, respectively. Let $C_{q_{(1)}}$ be the output of the above steps to find the set of candidate relative-distance representations on Q with the starting point $q_{(1)}$. If $dist(Q, P) \leq \delta$, then there exist three points $q_{(2)}, q_{(3)}$ and $q_{(4)}$ in Q, such that $p_{(i)}$ is the correspondence point of $q_{(i)}$ on P for $i \in [2, 4]$, and $rd(q_{(1)}|q_{(2)}, q_{(3)}, q_{(4)}) \in C_{q_{(1)}}$.*

PROOF SKETCH. Since $dist(Q, P) \leq \delta$, by Lemma 4.1, for $i \in [2, 4]$, $q_{(i)}$ exists in P, and $\|q_{(i)}, p_{(i)}\| \leq \triangle$. $S_{(i)}$ for $i \in [2, 4]$ must contain $q_{(i)}$ by our steps of finding $S_{(i)}$. Clearly, $rd(q_{(1)}|q_{(2)}, q_{(3)}, q_{(4)})$ will be included in the result set $C_{q_{(1)}}$. □

4.3 Two Phases of C_2O

We present the preprocessing phase and the query phase of C_2O in Section 4.3.1 and Section 4.3.2, respectively.

4.3.1 Preprocessing Phase. The preprocessing phase is straightforward with our donut representation. It involves the following steps. For each point cloud P in $\mathcal{P}$, we do the following sub-steps. The first sub-step is to build a 3D index I_P (e.g., R*-tree [3]) on all points in P. The second sub-step is to perform the following procedure for each point $p_{(1)}$ in P. We construct the relative-distance representation of $p_{(1)}$ (i.e., $rd(p_{(1)}|p_{(2)}, p_{(3)}, p_{(4)})$ where $p_{(2)}, p_{(3)}$ and $p_{(4)}$ are the other three points found (as described before) with the help of index I_P. We insert $rd(p_{(1)}|p_{(2)}, p_{(3)}, p_{(4)})$ into a 6-dimensional index I_{DB} (e.g., R*-tree), initialized to an empty index. Note that in this index, each $rd(p_{(1)}|p_{(2)}, p_{(3)}, p_{(4)})$ is associated with two parts: (1) the ID of the point cloud P in $\mathcal{P}$ and (2) the point IDs of $p_{(1)}, p_{(2)}, p_{(3)}$ and $p_{(4)}$.

It is easy to observe that the final index size of I_{DB} is $O(n)$. Next, we discuss the preprocessing time. Firstly, the time complexity of building an index I_P of one point cloud P is $O(|P| \log |P|)$, and the total time complexity of building indices of all point clouds will be $O(n \log n)$ since $|P|$ is at most n. Secondly, for each point in a database point cloud, we obtain the relative-distance representation in expected $O(\log |P|)$ time with the help of I_P. Since there are n database points, obtaining all relative-distance representations takes $O(n \log n)$ time. The overall preprocessing time complexity is $O(n \log n)$.

4.3.2 Query Phase. We describe the following 2 steps of our query phase as follows. Consider a query point cloud Q.

Step 1 (Relative-Distance Representation Candidate Generation): Firstly, we randomly find a point $q_{(1)}$ from Q. Note that in our implementation, we select a point q in Q not near to the "boundary" of point cloud Q because we want to construct the tetrahedron from q with sufficient points in the proximity of q (since otherwise, there are no points to be chosen to construct a "regular" tetrahedron from a boundary point in Q). Secondly, we perform the steps described in Section 4.2 and obtain a set $C_{q_{(1)}}$ of candidate relative-distance representations.

Step 2 (Point Cloud Matching): We first initialize a variable $\mathcal{R}$, which is a set of IDs of the point clouds in P storing the results of the query found, to an empty set. Then, we do the following steps. *Step a:* We initialize a variable C, which is to store a set of 2-tuples each in the form of (R_Q, R_P) where R_Q (R_P) is a relative-distance representation of a point in Q (P), to an empty set. *Step b:* For each representation R_Q in $C_{q_{(1)}}$, We perform a window query on I_{DB} where the query point in this query is R_Q and the query range is $2\triangle$, and obtain a result X which is a set of relative-distance representations in I_{DB}. Note that each representation R_P in X is associated with (1) an ID i and (2) the point IDs of the 4 owners of this representation R_P. Then, for each R_P in X, we insert a 2-tuple (R_Q, R_P) into C. *Step c:* For each (R_Q, R_P) in C, we perform the following step. Firstly, let i be the ID of R_P. Secondly, if i could be found in $\mathcal{R}$, we do nothing (since there is no need to process R_P because the ID of its point cloud P is in the result $\mathcal{R}$). Otherwise (i.e., if i could not be found in $\mathcal{R}$), we do the following. We perform a coarse transformation Θ based on (1) the 4 owners of R_Q and (2) the 4 owners of R_P. Then, based on Θ, we perform a complete transformation Θ_o based on (1) all points of Q and (2) all points of point cloud P with ID i. If $dist_{diff}(Q, P|\Theta_o) \leq \delta$, then we insert the ID i into $\mathcal{R}$.

The following theorem shows the correctness of C_2O.

Theorem 4.1. *We are given a query point cloud Q and a non-negative real number δ. Let $\mathcal{R}$ be the set of database point clouds returned by our original query phase. Let $\mathcal{R}^*$ be the optimal solution of our 3D object retrieval problem. Then, $\mathcal{R} = \mathcal{R}^*$.*

Proof sketch. We need to show that $\mathcal{R}$ contains no false positive or false negative. The former is obvious since we only output P such that $dist(Q, P) \leq \delta$. For the latter, for any $P \in R^*$, there exists a 2-tuple (R_Q, R_P) in $C_{q_{(1)}}$ such that R_P and P has the same ID (by Lemma 4.2), and (R_Q, R_P) will finally give $dist(Q, P) \leq \delta$. □

5 RELATED WORK

We first describe the relevancy to existing problems and the relevancy to existing algorithms.

Relevancy to Existing Problems: As described in Section 1, our 3D object retrieval problem is closely related to registration [2, 9, 15, 16, 22, 32]. It is also related to *similarity search* [6, 21, 36, 40], *pattern matching* [5, 10, 14] and *object detection* [8, 29, 43] though there are some differences. In the literature, similarity search, also known as *shape matching*, is to find a number of 3D point clouds in a 3D scene which "look" similar to a general object (e.g., chair). However, since this existing problem does not provide a *concrete*

similarity measurement, the 3D point clouds returned in the output may not really be a chair. Pattern matching can be regarded as one special case of our problem when there is *only one* point cloud in the database and one query point cloud and the distance function used in this work is replaced by our distance function. Object detection is to find a set of objects in the 3D point cloud with models like deep-learning models which require some "labelled" datasets containing some objects "manually" marked as objects. However, object detection does not involve any query point cloud in its problem which is fundamentally different from us.

Relevancy to Existing Algorithms:

Although no existing algorithms solve our 3D object retrieval problem exactly, there are some existing algorithms which can be adapted to our problem. They are *Super4PCS* [23] and *Go-ICP* [39].

Super4PCS adopts the well-known *4-point co-planar matching* scheme [2] to find the best transformation between two point clouds. It involves three steps, namely (1) the point-pair retrieval step (which is to find two random point pairs from Q, forming a 4-point structure Ψ, and to find a set S_1 of point pairs from P with pairwise distance equal to one of the random point pairs and another set S_2 of point pairs from P with pairwise distance equal to the other random point pair), (2) the 4-point structure search step (which, for each point pair in S_1 and each point pair in S_2, is to construct a 4-point structure based on these 2 point pairs and to insert this structure to a variable F if this structure is "similar" to Ψ) and (3) the transformation verification step (which, for each structure Φ in F, is to perform a coarse transformation on Ψ (for matching the space of Φ) and then to perform a locally optimized transformation on the *entire* point cloud Q (containing Ψ) (for matching the space of the database point cloud containing Φ) by a method like ICP [31]). Note that *Super4PCS* returns locally-optimized transformations only (not necessarily globally optimal transformation).

Go-ICP can be regarded as the state-of-the-art algorithm to find the *globally optimal* transformation between two point clouds. In *Go-ICP*, each transformation is represented by six parameters and thus, the search space considered is the space containing all possible values from these parameters. It searches for the best transformation in this search space by a Branch-and-bound search strategy. However, *Go-ICP* is costly, with $O(8^l)$ time complexity where l is a data-dependent parameter (and is about 30 on average in our experiment). Note that although the original Go-ICP has high time cost, it will become much more efficient if an initial transformation Θ close to the optimal is first given. This is because, with Θ, *Go-ICP* could find the exact optimal transformation by a fast sub-procedure.

We adapt *Super4PCS* [23] and *Go-ICP* [39] as follows.

(1) **Super4PCS-Adapt(NoIndex):** We modify *Super4PCS* to form our deterministic approach as follows. Firstly, in the 4-point structure search step, we replace the heuristic error parameter by $\triangle$ (the upper bound of the correspondence distance for all query points) for determining whether two 4-point structures are "similar". Secondly, in the transformation verification step, after obtaining the coarse transformation results, we run our complete transformation and object retrieval steps of our C_2O algorithm for global optimality. Thirdly, since *Super4PCS* handles two point clouds only, we run our adapted algorithm between the query and each database point cloud. (2) **Super4PCS-Adapt(Index):** Based on **Super4PCS-Adapt(NoIndex)**, we enhance the point-pair retrieval step by

introducing a one-dimensional index (e.g., B+-tree) to index all pairwise distances among all points in each database point cloud. Note that in all steps of **Super4PCS-Adapt(NoIndex)**, the only step we could improve with the index is the point-pair retrieval step and the improvement is based on the pairwise distance search (which leads us to propose to introduce a one-dimensional index). With this index, the two sets (i.e., S_1 and S_2) could be found more efficiently. (3) **GoICP-Adapt**: We also consider a trivial adaptation of *Go-ICP*. Since *Go-ICP* only gives the *optimal* transformation between two point clouds, we run *Go-ICP* for the query and each database point cloud. For each result, if the optimal distance is within δ, we include the corresponding database point cloud in the result set.

The non-index approach (i.e., **Super4PCS-Adapt(NoIndex)**) does not perform well (compared with our C_2O algorithm) because the 4-point search time cost is linear to the database size [23], but C_2O just takes $O(\log n + k_2)$ where k_2 is the size of the output. The index approach (i.e., **Super4PCS-Adapt(Index)**) does not perform well either (compared with C_2O) because the acceleration by the 1D index only affects the point-pair retrieval step, and the remaining steps for finding the matched 4-points are still time-consuming. Since the output size from the index could be as large as the database size, this algorithm are not efficient enough. Note that in our C_2O query phase, we have a similar step of finding all the relative-distance representations in the database. Our step only takes $O(\log n + k_2)$ time, where k_2 is very small and is equal to 40 on average in our experiment. The rationale of our improvement is that we represent and match a 4-point as a *whole* instead of handling it as two *separate* point-pairs in existing approaches. Finally, **GoICP-Adapt** does not perform well due to its high computation cost.

There are some existing algorithms solving the similarity search problem. They are PointNetVLAD [36], PCAN [40], feature-based descriptors [6, 34] and 3D shape contexts [21]. Two representative algorithms are PointNetVLAD [36] and PCAN [40] which are deep learning models trained on a number of 3D point clouds and are used to find the query point cloud efficiently with the trained deep learning models via embedding vectors as described in Section 1. However, both models do not consider any rotation/translation of the given query point cloud and thus, the results from these models are not accurate. To improve their accuracy, we adapt the *training* phase of each of these two models as follows. Given a training query point cloud, they need to find and label all the similar database point clouds to form training samples. To obtain this, we apply our distance measurement instead of their original similarity measurement. Moreover, methods of feature-based descriptors [6, 34] form a *local descriptor* (which could be represented in the form of histogram) measuring some geometric features of neighboring points (e.g., the pairwise distances among these points) for each of the sampled key points from a point cloud, and finally match two point clouds with similar local descriptors. Unfortunately, they still give inaccurate results since the descriptors are easily affected by noise and two key point sets (which are *subsets* of the entire point clouds) with the same local descriptors cannot be guaranteed for two similar (entire) point clouds. Methods of 3D shape contexts [21] summarize a global descriptor from the above local descriptors of key points for a similarity search, and thus they still suffer from the same issues as feature-based descriptors.

6 EXPERIMENT

6.1 Setup

We conducted experiments on a machine with 2.66GHz CPU and 48G memory. The programming language is C++ without any CPU- or GPU-level parallelization.

6.1.1 Datasets. We used the well-structured 3D object dataset repository called *redwood* [1] (because this database is commonly used in the literature of 3D graphics [11, 12, 28]). We used two datasets from this repository, namely *Object* [12] and *Indoor* [28]. Dataset *Object* involves 441 3D objects each of which has a small point cloud, and dataset *Indoor* involves 5 scenes (or formally objects in our context) in an indoor environment each of which has a large point cloud. In dataset *Object*, following the setting of [26, 30, 38], for each object, we form a point cloud of size around 100 using quadric edge collapse decimation [35] (a seminal method implemented in MeshLab [13]). The diameter of the minimum bounding sphere covering each point cloud (simply called the *diameter* of this point cloud) is 3,000–6,000mm. We randomly chose 400 objects in dataset *Object* to form a new database dataset called *Object-DB*, serving for the database purpose, and chose the remaining 41 objects to form a new dataset *Object-OutsideDB* which will be used in the query generation (to be described later). In dataset *Indoor*, we chose three scenes which are bedroom, boardroom and loft to form a new database dataset called *Indoor-DB* and chose the remaining 2 scenes to form a new dataset *Indoor-OutsideDB*. The total database size is 10 million. The diameter of each point cloud is approximately 250,000mm.

Based on the database datasets, we would like to construct additional datasets for scalability test. Thus, for each of these 2 datasets, we construct additional datasets as follows. In dataset *Object-DB*, we create 5 datasets, namely *Object #1*, *Object #2*, *Object #3*, *Object #4* and *Object #5*, with the number of objects as 100, 1K, 10K, 100K and 1M , respectively. For the first dataset, we use 100 (out of 400) objects from dataset *Object-DB*. For the remaining 4 datasets, we generate them as follows. Since each of these datasets contains more than 400 objects, we generate additional objects with the following steps. We pick one object (or point cloud) P from the original dataset (i.e., *Object*) and create a new object by perturbing the coordinates of each point in P with distortion values generated according to Gaussian distribution with mean equal to 0 and standard deviation equal to 0.05 times the diameter of point cloud P. The sizes of the 5 generated datasets (i.e., n) in *Object-DB* are 12.2K, 118K, 1.18M, 11.8M and 117M, respectively. In dataset *Indoor-DB*, we create 3 datasets, namely *Indoor #1*, *Indoor #2* and *Indoor #3* with database size as 10K, 100K and 1M. Since each of these 3 datasets is much smaller than dataset *Indoor-DB*, we sample all point clouds in dataset *Indoor-DB* using quadric edge collapse decimation [35] such that the database size of each of these 3 datasets is equal to the desired size. We then re-scale the three datasets to their diameters around 10,000mm, 30,000mm and 80,000mm, respectively, such that the average point-pairwise distance of each dataset is similar to that of dataset *Indoor-DB*. We also call dataset *Indoor-DB* as *Indoor #4*.

6.1.2 Random Query Generation. We generated random queries with 5 types. The first-type queries are generated according to objects from the database. Specifically, in each dataset generated from dataset *Object-DB*, we randomly pick one point cloud out of all the

database objects as the query point cloud. In each dataset generated from dataset *Indoor-DB*, we select one scene randomly from the 3 scene point clouds and extract a random part from the selected scene as the query point cloud with diameter roughly equal to the target diameter as 1,000mm. We also vary this extraction diameter to 1,500mm, 2,000mm, 2,500mm and 3,000mm for our scalability tests. After obtaining the query point cloud, we transform it by a random translation and rotation. In order to simulate different levels of noise, we also introduce noise to 10%, 20%, 30% and 40% of the query point cloud by performing a perturbation on each coordinate value of the point cloud following Gaussian distribution with mean equal to 0 and standard deviation equal to 0.0025 times the query point cloud diameter [42]. The second-type queries are generated according to objects outside the database. Specifically, for experiments related to *Object* (*Indoor*), we randomly pick one point cloud from dataset *Object-OutsideDB* (*Indoor-OutsideDB*) as the query point cloud. Then, we perform random transformation and noise perturbation similar to the first type of queries. The third-, fourth- and fifth-type queries are generated according to different distributions of the first- and second-type queries. The third-type (fourth-type) queries are generated from 80% (20%) first-type queries and 20% (80%) second-type queries. The fifth-type queries are generated from 50% first-type queries and 50% second-type queries. In the following, by default, we use the first-type queries for experiments. We use other types of queries for other specified experiments.

6.1.3 Algorithms. We include all the adapted existing algorithms (described in Section 5) for comparison: **Super4PCS-Adapt(NoIndex)** [23], **Super4PCS-Adapt(Index)** [23] and **GoICP-Adapt** [39]. Our proposed algorithm is denoted by C_2O. In addition, we include the two state-of-the-art deep learning algorithms for comparison, denoted as **PointNetVLAD** [36] and **PCAN** [40]. Note that both algorithms do not guarantee accurate results, and thus we will measure their F-measure values.

For each database/query point cloud, we build an R*-tree for some spatial queries like nearest neighbor queries and range queries (used in our proposed algorithm and our compared algorithms). Following the pre-processing steps of the deep learning algorithms [36, 40], we split each database point cloud of dataset Indoor into a number of small point clouds using a voxel grid [17] of grid size equal to our default query diameter (to be introduced later) where each small point cloud (containing all the points within a cell) represents a portion of a database point cloud. For some experiments where the query diameter is varied for dataset Indoor, we set the grid size to different values accordingly to form different pre-processed Indoor datasets. Moreover, in the implementation of [36, 40], a retrieved portion is marked correct if its center has its Euclidean distance to the center of the optimal portion within a value approximately equal to half the largest side length of the bounding box of the query point cloud (that is, it is very close to the optimal portion). Thus, in our experiments for dataset Indoor, we adopt a similar setting that a portion is regarded as the correct query result if the Euclidean distance from its center to the center of an optimal portion is at most half the query diameter. Furthermore, since the deep learning algorithms are designed to retrieve the most similar objects (or portions) in the database, we return the top-k among all database point clouds (or portions) for the deep learning algorithms

where k is set to the number of all the optimal database point clouds (or portions) for a given query and δ. Due to the architecture nature of the deep learning algorithms requiring 128 points as input, we re-sample each database/query object (or portion) with exactly 128 points using quadric edge collapse decimation.

6.1.4 Factors. We vary the following factors: (1) r, (2) query point cloud size, (3) database size, (4) δ and (5) query noise percentage. (1) By default, when we vary other factors, we set r to 1,200mm and 350mm for dataset *Object* and dataset *Indoor*, respectively (since this setting gives the best (i.e., smallest) query time). (2) The default query point cloud diameter for dataset *Indoor* is 1000mm. Note that different from dataset *Indoor-DB*, there is no need to vary query point cloud diameter for dataset *Object-DB* since a whole database object is specified as a query object. (3) The default dataset size is 118K (10K) when we do experiments for datsets generated from *Object* (*Indoor*). That is, by default, we used dataset *Object #2* (*Indoor #1*). (4) Following [39], we set the default value of δ to be 3.2% (of the query object diameter). (5) The default query noise percentage (as described in Section 6.1.2) is 10%.

6.1.5 Measurements. We have the following measurements: (1) the index building time, (2) the index size, (3) the query time, (4) the number of complete transformations and (5) the F-measure (showing how accurate the algorithms are). All measurements are straightforward. Note that the F-measure is defined to be the harmonic mean of the precision and recall of a query execution, where the precision is defined to be the proportion of the correct results retrieved by an algorithm (i.e., the true positives) over all the retrieved results, and the recall is defined to be the proportion of the retrieved correct results over all the correct results. Each measurement is reported as an average of at least 100 random query executions.

6.2   Results

We show our experimental results in the following parts. Firstly, we study the design of our C_2O algorithm (Section 6.2.1). Next, we compare our C_2O algorithm with some other algorithms in dataset *Object* (Section 6.2.2). After that, we show the results in dataset *Indoor* (Section 6.2.3).

6.2.1 Study of Design of Our C_2O Algorithm. We conducted experiments about the design of C_2O (e.g., choosing the best value of r (based on the smallest query time), choosing the regular tetrahedron (based on the high pruning power) and studying the effectiveness of pruning relative-distance representations with a multi-dimensional index I_{DB}). See Section D.1 for details.

6.2.2 Comparison Among All Algorithms in dataset Object. In the following, we give the experimental results on dataset *Object*.

Study of Algorithms Which Need Preprocessing: We study the preprocessing time and the memory consumption of index-based algorithms (i.e., C_2O and **Super4PCS-Adapt(Index)**) and deep learning algorithms (i.e., **PointNetVLAD** and **PCAN**). The preprocessing time and the memory consumption of an index-based algorithm (a deep learning algorithm) refer to its index construction time (training time) and its index size (deep learning model size), respectively. As shown in Figure 8(a), the preprocessing times of all algorithms increase with the number of database objects. Though
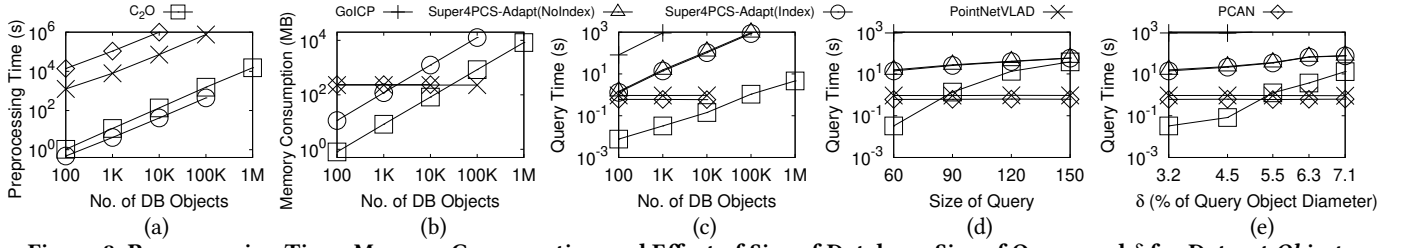
Figure 8: Preprocessing Time, Memory Consumption and Effect of Size of Database, Size of Query and δ for Dataset *Object*

Super4PCS-Adapt(Index) has a slightly shorter preprocessing time than C_2O, **Super4PCS-Adapt(Index)** occupies the largest memory such that it could not be executed on the dataset containing 1M database objects (as shown in Figure 8(b)). Figure 8(b) shows that the memory consumption of index-based algorithms increases with the number of database objects but the memory consumption of deep learning algorithms remains unchanged (since their model sizes are independent of the number of database objects).

Effect of Size of Database: The query time of all non-deep learning algorithms increases with the number of database objects as shown in Figure 8(c). Our C_2O has the shortest query time (e.g., 4.6s when there are 1M database objects). However, the fastest baseline algorithm **Super4PCS-Adapt(Index)** has 2–3 orders of magnitude longer query time than C_2O, although it slightly improves **Super4PCS-Adapt(NoIndex)** due to its index. **GoICP-Adapt** takes the longest query time due to its costly optimal transformation for all database objects. Note that the query times of the two deep learning algorithms (i.e., **PointNetVLAD** and **PCAN**) remain nearly unchanged at around 0.6s because the time of searching the embedding vectors of all database objects in the K-D tree is very small and the increase in the search time is insignificant even with an increase of the number of database objects due to the efficient search of the K-D tree. Nevertheless, in our default setting when there are 1K objects, the query time of our algorithm C_2O is still much smaller (i.e., 0.032s) than deep learning algorithms. Later, we will show that the results of deep learning algorithms are inaccurate.

Effect of Size of Query: Figure 8(d) shows that the query times of all algorithms except deep learning algorithms increase with the size of the query. When the size of query increases, the parameter $\triangle$ ($= \delta|Q|^{1/2}$ where $|Q|$ is the query size) also increases, resulting in increased query time for our algorithm and **Super4PCS**-related algorithms. The query times of deep learning algorithms remain unchanged due to re-sampling to 128 points as input to their models for every query.

Effect of δ: Figure 8(e) shows that the query times of all algorithms except deep learning algorithms increase with δ. Our C_2O still outperforms all the non-deep learning algorithms.

Effect of Noise Percentage: Our results show that the noise percentage does not affect the query time of all algorithms, and C_2O still gives the smallest query time. The F-measure of all algorithms except deep learning algorithms is 100% but that of deep learning algorithms is only around or less than 15%. See Section D.2 for details.

Case Study: We conducted a number of case studies about the results returned by our proposed algorithm (i.e., C_2O) and the deep learning algorithms. As shown in Figure 1, given the query point cloud, C_2O returns Object 1, 2 and 3 as the similar objects under a default setting. However, **PointNetVLAD** returns an irrelevant object (i.e., a car shown as Object 4) under the same setting. We also conducted case studies on other query objects (e.g., bench and standing sign) with different noise percentages (e.g., 40%). We have similar results. Note that the other deep learning algorithm **PCAN** gives similar inaccurate results. See Section D.2 for details.

Results for Other Query Types: We conducted experiments with other types of queries as described in Section 6.1.2 (i.e., the second-, third-, fourth- and fifth-type queries). We obtained similar experimental results. It is worth mentioning that the query time of C_2O on the queries involving more objects outside the database (i.e., the second- and fourth-type queries) are slightly larger than those on other queries (because more database objects have to be processed to find similar objects). But, the query times are all within 11.6s for C_2O (even on 1M database objects). See Section D.2 for details.

6.2.3 Query Results for Dataset Indoor.
We also conducted experiments on dataset *Indoor*. We also obtained similar experimental results. When the database size is 1M which is the largest database size such that the non-deep learning baseline algorithms can run the query results in reasonable time (i.e., within 1000s), the query time of our proposed algorithm is within 4.1s but those of the baseline algorithms other than deep learning algorithms are at least 657s. The F-measure of our proposed algorithm is 100% but the F-measure of deep learning algorithms are only less than 15%. See Section D.3 for details.

6.2.4 Summary of Experimental Results.
We verify the superior efficiency of our proposed C_2O algorithm for object retrieval queries, which generally outperform the existing accurate algorithms by 1-3 orders of magnitude for various experimental configurations. In dataset *Object* containing over 1M objects (more than 100M points), our algorithm obtains efficient and superior performance (e.g., within 5 seconds), while none of the existing accurate algorithms handle it in reasonable time (e.g., less than 1000 seconds). Moreover, our algorithm returns accurate results with 100% F-measure value, but the existing deep learning algorithms obtain at most around 15% F-measure value.

7 CONCLUSION

In this paper, we studied the problem about efficient 3D object retrieval which have many applications. We propose our C_2O algorithm, which, in most of our experiments, performs up to 1−2 orders of magnitude faster than all adapted algorithms in the literature. Moreover, C_2O guarantees 100% accurate results but some adapted algorithms do not. Some possible future work could be the top-k version and the dynamic version of 3D object retrieval.

REFERENCES

[1] 2022. http://redwood-data.org/

[2] Dror Aiger, Niloy J Mitra, and Daniel Cohen-Or. 2008. 4-points congruent sets for robust pairwise surface registration. In *ACM transactions on graphics (TOG)*, Vol. 27. Acm, 85.

[3] Norbert Beckmann, Hans-Peter Kriegel, Ralf Schneider, and Bernhard Seeger. 1990. The R*-tree: an efficient and robust access method for points and rectangles. In *Acm Sigmod Record*, Vol. 19. Acm, 322–331.

[4] Paul J Besl and Neil D McKay. 1992. Method for registration of 3-D shapes. In *Sensor fusion IV: control paradigms and data structures*, Vol. 1611. International Society for Optics and Photonics, 586–606.

[5] Peter Brass. 2000. Exact point pattern matching and the number of congruent triangles in a three-dimensional pointset. In *European Symposium on Algorithms*. Springer, 112–119.

[6] Benjamin Bustos, Daniel A Keim, Dietmar Saupe, Tobias Schreck, and Dejan V Vranić. 2005. Feature-based similarity search in 3D object databases. *ACM Computing Surveys (CSUR)* 37, 4 (2005), 345–387.

[7] Chu-Song Chen, Yi-Ping Hung, and Jen-Bo Cheng. 1999. RANSAC-based DARCES: A new approach to fast automatic registration of partially overlapping range images. *IEEE Transactions on Pattern Analysis and Machine Intelligence* 21, 11 (1999), 1229–1234.

[8] Xiaozhi Chen, Huimin Ma, Ji Wan, Bo Li, and Tian Xia. 2017. Multi-view 3d object detection network for autonomous driving. In *Proceedings of the IEEE Conference on Computer Vision and Pattern Recognition*. 1907–1915.

[9] Yang Chen and Gérard Medioni. 1992. Object modelling by registration of multiple range images. *Image and vision computing* 10, 3 (1992), 145–155.

[10] L Paul Chew, Michael T Goodrich, Daniel P Huttenlocher, Klara Kedem, Jon M Kleinberg, and Dina Kravets. 1997. Geometric pattern matching under Euclidean motion. *Computational Geometry* 7, 1-2 (1997), 113–124.

[11] Sungjoon Choi, Qian-Yi Zhou, and Vladlen Koltun. 2015. Robust reconstruction of indoor scenes. In *Proceedings of the IEEE Conference on Computer Vision and Pattern Recognition*. 5556–5565.

[12] Sungjoon Choi, Qian-Yi Zhou, Stephen Miller, and Vladlen Koltun. 2016. A large dataset of object scans. *arXiv preprint arXiv:1602.02481* (2016).

[13] Paolo Cignoni, Marco Callieri, Massimiliano Corsini, Matteo Dellepiane, Fabio Ganovelli, and Guido Ranzuglia. 2008. Meshlab: an open-source mesh processing tool.. In *Eurographics Italian chapter conference*, Vol. 2008. 129–136.

[14] Pedro Jussieu de Rezende and DT Lee. 1995. Point Set pattern matching ind-dimensions. *Algorithmica* 13, 4 (1995), 387–404.

[15] Jianmin Dong, Zhongmin Cai, and Shaoyi Du. 2016. Improvement of affine iterative closest point algorithm for partial registration. *IET Computer Vision* 11, 2 (2016), 135–144.

[16] Gil Elbaz, Tamar Avraham, and Anath Fischer. 2017. 3D point cloud registration for localization using a deep neural network auto-encoder. In *Proceedings of the IEEE Conference on Computer Vision and Pattern Recognition*. 4631–4640.

[17] James D Foley, Andries van Dam, John F Hughes, and Steven K Feiner. 1990. Spatial-partitioning representations; Surface detail. *Computer Graphics: Principles and Practice* (1990).

[18] Andreas Geiger, Philip Lenz, and Raquel Urtasun. 2012. Are we ready for autonomous driving? the kitti vision benchmark suite. In *2012 IEEE Conference on Computer Vision and Pattern Recognition*. IEEE, 3354–3361.

[19] Aleksey Golovinskiy, Vladimir G Kim, and Thomas Funkhouser. 2009. Shape-based recognition of 3D point clouds in urban environments. In *2009 IEEE 12th International Conference on Computer Vision*. IEEE, 2154–2161.

[20] Leonid Keselman, John Iselin Woodfill, Anders Grunnet-Jepsen, and Achintya Bhowmik. 2017. Intel (r) realsense (tm) stereoscopic depth cameras. In *2017 IEEE Conference on Computer Vision and Pattern Recognition Workshops (CVPRW)*. IEEE, 1267–1276.

[21] Marcel Körtgen, Gil-Joo Park, Marcin Novotni, and Reinhard Klein. 2003. 3D shape matching with 3D shape contexts. In *The 7th central European seminar on computer graphics*, Vol. 3. Citeseer, 5–17.

[22] Hongdong Li and Richard Hartley. 2007. The 3D-3D registration problem revisited. In *2007 IEEE 11th international conference on computer vision*. IEEE, 1–8.

[23] Nicolas Mellado, Dror Aiger, and Niloy J Mitra. 2014. Super 4pcs fast global pointcloud registration via smart indexing. In *Computer Graphics Forum*, Vol. 33. Wiley Online Library, 205–215.

[24] Mustafa Mohamad, Mirza Tahir Ahmed, David Rappaport, and Michael Greenspan. 2015. Super generalized 4pcs for 3d registration. In *2015 International Conference on 3D Vision*. IEEE, 598–606.

[25] Mustafa Mohamad, David Rappaport, and Michael Greenspan. 2014. Generalized 4-points congruent sets for 3d registration. In *2014 2nd international conference on 3D vision*, Vol. 1. IEEE, 83–90.

[26] Adithyavairavan Murali, Arsalan Mousavian, Clemens Eppner, Chris Paxton, and Dieter Fox. 2020. 6-dof grasping for target-driven object manipulation in clutter. In *2020 IEEE International Conference on Robotics and Automation (ICRA)*. IEEE, 6232–6238.

[27] Alain Pagani, Christiano Couto Gava, Yan Cui, Bernd Krolla, Jean-Marc Hengen, and Didier Stricker. 2011. Dense 3D Point Cloud Generation from Multiple High-resolution Spherical Images.. In *VAST*. 17–24.

[28] Jaesik Park, Qian-Yi Zhou, and Vladlen Koltun. 2017. Colored point cloud registration revisited. In *Proceedings of the IEEE International Conference on Computer Vision*. 143–152.

[29] Charles R Qi, Wei Liu, Chenxia Wu, Hao Su, and Leonidas J Guibas. 2018. Frustum pointnets for 3d object detection from rgb-d data. In *Proceedings of the IEEE Conference on Computer Vision and Pattern Recognition*. 918–927.

[30] Charles R Qi, Li Yi, Hao Su, and Leonidas J Guibas. 2017. Pointnet++: Deep hierarchical feature learning on point sets in a metric space. *arXiv preprint arXiv:1706.02413* (2017).

[31] Szymon Rusinkiewicz and Marc Levoy. 2001. Efficient variants of the ICP algorithm. In *3dim*, Vol. 1. 145–152.

[32] Radu Bogdan Rusu, Nico Blodow, and Michael Beetz. 2009. Fast point feature histograms (FPFH) for 3D registration. In *2009 IEEE International Conference on Robotics and Automation*. IEEE, 3212–3217.

[33] Radu Bogdan Rusu, Nico Blodow, Zoltan Marton, Alina Soos, and Michael Beetz. 2007. Towards 3D object maps for autonomous household robots. In *2007 IEEE/RSJ International Conference on Intelligent Robots and Systems*. IEEE, 3191–3198.

[34] Radu Bogdan Rusu, Nico Blodow, Zoltan Csaba Marton, and Michael Beetz. 2008. Aligning point cloud views using persistent feature histograms. In *2008 IEEE/RSJ International Conference on Intelligent Robots and Systems*. IEEE, 3384–3391.

[35] Marco Tarini, Nico Pietroni, Paolo Cignoni, Daniele Panozzo, and Enrico Puppo. 2010. Practical quad mesh simplification. In *Computer Graphics Forum*, Vol. 29. Wiley Online Library, 407–418.

[36] M. A. Uy and G. H. Lee. 2018. PointNetVLAD: Deep Point Cloud Based Retrieval for Large-Scale Place Recognition. In *Proceedings of the IEEE Conference on Computer Vision and Pattern Recognition (CVPR)*.

[37] D Van Krevelen and R Poelman. 2007. Augmented reality: Technologies, applications, and limitations. *Vrije Univ. Amsterdam, Dep. Comput. Sci* (2007).

[38] Danfei Xu, Dragomir Anguelov, and Ashesh Jain. 2018. Pointfusion: Deep sensor fusion for 3d bounding box estimation. In *Proceedings of the IEEE Conference on Computer Vision and Pattern Recognition*. 244–253.

[39] Jiaolong Yang, Hongdong Li, and Yunde Jia. 2013. Go-icp: Solving 3d registration efficiently and globally optimally. In *Proceedings of the IEEE International Conference on Computer Vision*. 1457–1464.

[40] Wenxiao Zhang and Chunxia Xiao. 2019. PCAN: 3D attention map learning using contextual information for point cloud based retrieval. In *Proceedings of the IEEE/CVF Conference on Computer Vision and Pattern Recognition*. 12436–12445.

[41] Zhengyou Zhang. 2012. Microsoft kinect sensor and its effect. *IEEE multimedia* 19, 2 (2012), 4–10.

[42] Qian-Yi Zhou, Jaesik Park, and Vladlen Koltun. 2016. Fast global registration. In *European Conference on Computer Vision*. Springer, 766–782.

[43] Yin Zhou and Oncel Tuzel. 2018. Voxelnet: End-to-end learning for point cloud based 3d object detection. In *Proceedings of the IEEE Conference on Computer Vision and Pattern Recognition*. 4490–4499.

A   TABLE OF NOTATIONS

In Table 1, we summarize the commonly used notations in this paper.

B   EXTENDED DETAILS OF ALGORITHM C_2O

B.1   Extended Details of Donut Representation

In Section 4.1, we introduced the steps of forming tetrahedron, which generate a tetrahedron close to a regular tetrahedron (represented by $p_{(1)}$, $p_{(2)}$, a and b). Now, we give a lemma to explicitly show that the tetrahedron represented by point $p_{(1)}$, $p_{(2)}$, a and b is a regular tetrahedron.

LEMMA B.1. *The tetrahedron represented by $p_{(1)}$, $p_{(2)}$, a and b is regular.*

PROOF. Since m is the mid-point between $p_{(1)}$ and $p_{(2)}$, $ma \perp mp_{(1)}$ and $\|ma\| = r' = \frac{\sqrt{3}}{2}\|p_{(1)}, p_{(2)}\|$, we could derive that $\triangle p_{(1)}ap_{(2)}$ is a regular triangle. Since point b is decided by rotating ma around point m inside the perpendicular plane of $mp_{(1)}$, it holds that $mb \perp mp_{(1)}$ and $\|m, a\| = \|m, b\|$. Similarly, we know that $\triangle p_{(1)}bp_{(2)}$ is also a regular triangle. It left to show that $\|a, b\| = \|p_{(1)}, p_{(2)}\|$ such that all the edges of tetrahedron formed by point $p_{(1)}$, $p_{(2)}$, a and b are equal. Since $\theta = \arccos 1/3$, by the law of cosines, it is easy to derive that $\|a, b\| = \sqrt{2r'^2 - 2r'^2 \cos\theta} = \frac{2\sqrt{3}}{3}r' = \|p_1, p_2\|$. □

B.2   Extended Details of Constructing $S_{(2)}$, $S_{(3)}$ and $S_{(4)}$

In this section, we give more detailed explanation of how we construct $S_{(2)}$, $S_{(3)}$ and $S_{(4)}$, which has been introduced in Section 4.2.1, Section 4.2.2 and Section 4.2.3, respectively.

We give the following lemma based on the concepts of the sphere bounding zone, which can help to construct $S_{(2)}$. The idea is that we would like to find a small subset of Q, denoted by $S_{(2)}$, which must contain the desired $q_{(2)}$ having $p_{(2)}$ as the correspondence point on P. Since $p_{(2)}$ is the nearest neighbor of the r-sized ball of $p_{(1)}$ in P (and is very close to the r-sized ball of $p_{(1)}$ in most cases), based on the two major principles, it is guaranteed that our desired $q_{(2)}$ is also close to the r-sized ball of $q_{(1)}$ or the distance from our desired $q_{(2)}$ to $q_{(1)}$ is close to the distance from $p_{(2)}$ to $p_{(1)}$.

LEMMA B.2. *Consider a query point cloud Q and a database point cloud P. Let $q_{(1)}$ be a point in Q whose correspondence point on P is $p_{(1)}$. Let $p_{(2)}$, $p_{(3)}$ and $p_{(4)}$ be the second, third and fourth owners of the relative-distance representation of $p_{(1)}$, respectively. Let $S_{(2)}$ be the set of all points from Q in $sbz(q_{(1)}, [r - 2\triangle, \|q_{(1)}, q'\| + 4\triangle])$ where $q' = ball\text{-}NN(q_{(1)}, r + 2\triangle|Q)$. If $dist(Q, P) \leq \delta$, then there exists a point $q_{(2)}$ in $S_{(2)}$ such that $p_{(2)}$ is the correspondence point of $q_{(2)}$ on P.*

PROOF SKETCH. Since $dist(Q, P) \leq \delta$, by Lemma 4.1, $q_{(2)}$ exists in Q. Then, we need to show $r - 2\triangle \leq \|q_{(1)}, q_{(2)}\| \leq \|q_{(1)}, q'\| + 4\triangle$. If not, then it must be contradicted to the definition of q' and $p_{(2)}$ and conditions $\|q_{(1)}, p_{(1)}\| \leq \triangle$ and $\|q_{(2)}, p_{(2)}\| \leq \triangle$. □

The full proof can be found in Section C.4.

According to the above lemma, given $q_{(1)}$ (whose correspondence point on P is $p_{(1)}$), we can find a set $S_{(2)}$ of *candidate* points in Q for $q_{(2)}$, such that $S_{(2)}$ must contain $q_{(2)}$ which has its correspondence point on P as $p_{(2)}$, where $p_{(2)}$ is the second owner of the relative-distance representation of $p_{(1)}$ and can be listed out.

Next, suppose that we are given $q_{(1)}$ and $q_{(2)}$ (whose correspondence points on P are $p_{(1)}$ and $p_{(2)}$, respectively). Following the same steps introduced in Section 4.1, we find the locus of a point, denoted by D, with distance to both $q_{(1)}$ and $q_{(2)}$ equal to $\|q_{(1)}, q_{(2)}\|$ (i.e., $D = donut(m, r', \mathbf{n})$, where m is the mid-point between $q_{(1)}$ and $q_{(2)}$, $r' = \frac{\sqrt{3}}{2}\|q_{(1)}, q_{(2)}\|$ and $\mathbf{n}$ is the vector from $q_{(2)}$ to $q_{(1)}$). Note that in Section 4.1, for the *database* point cloud P, the third owner selected for the relative-distance representation of $p_{(1)}$ (i.e., $p_{(3)}$) is the nearest point in P to a donut (constructed based on the points in P). For this *query* point cloud Q, we also have a similar mechanism for finding the third point in Q. Based on the property that the distance from each query point to its correspondence point can be bounded (by Lemma 4.1), we use our defined concept in Section 4.2.2 called donut boundary zone to capture this property. We show the following lemma for constructing $S_{(3)}$ with the donut D derived from $q_{(1)}$ and $q_{(2)}$.

LEMMA B.3. *Consider a query point cloud Q and a database point cloud P. Let $p_{(2)}$, $p_{(3)}$ and $p_{(4)}$ be the second, third and fourth owners of the relative-distance representation of point $p_{(1)}$ in P, respectively. Let $q_{(1)}$ and $q_{(2)}$ be the points in Q whose correspondence point on P are $p_{(1)}$ and $p_{(2)}$, respectively. Let m be the mid-point between $q_{(1)}$ and $q_{(2)}$, $r' = \frac{\sqrt{3}}{2}\|q_{(1)}, q_{(2)}\|$, and $\mathbf{n}$ be the vector from $q_{(2)}$ to $q_{(1)}$. Let $D = donut(m, r', \mathbf{n})$ and $q' = donut\text{-}NN(m, r', \mathbf{n}|Q)$. Let $S_{(3)}$ be the set of all points from Q in $dbz(D, [0, dist(q', D) + 4\triangle])$. If $dist(Q, P) \leq \delta$, then there exists a point $q_{(3)}$ in $S_{(3)}$ such that $p_{(3)}$ is the correspondence point of $q_{(3)}$ on P.*

PROOF. Since $dist(Q, P) \leq \delta$, by Lemma 4.1, $q_{(3)}$ exists in Q. Since q' is the nearest point in Q to D, no points in Q is inside $dbz(D, [0, dist(q', D))$ (which does not include the points with distance to D exactly $dist(q', D)$), thus we only need to show that $dist(q_{(3)}, D) \leq dist(q', D) + 4\triangle$. Suppose $dist(q_{(3)}, D) > dist(q', D) + 4\triangle$, there exists point $p' \neq p_{(3)}$ in P, such that p' has smaller distance to D_p (the donut we build for P) than $p_{(3)}$, which contradicts that $p_{(3)}$ is the nearest point to D_p. □

According to the above lemma, given $q_{(1)}$ and $q_{(2)}$ (whose correspondence points on P are $p_{(1)}$ and $p_{(2)}$, respectively), we can also find a set $S_{(3)}$ of *candidate* points in Q for $q_{(3)}$ inside region $dbz(D, [0, dist(q', D) + 4\triangle])$ such that $S_{(3)}$ must contain $q_{(3)}$ which has its correspondence point on P as $p_{(3)}$, where $p_{(3)}$ is the third owner of the relative-distance representation of $p_{(1)}$ and can be listed out.

Finally, if we are given $q_{(1)}$, $q_{(2)}$ and $q_{(3)}$ (whose correspondence points on P are $p_{(1)}$, $p_{(2)}$ and $p_{(3)}$, respectively), we still follow the steps in Section 4.1 to find point a (a point on donut D that is nearest to $q_{(3)}$) and point b (the point at the position closest to a in the anti-clockwise direction from a on D in the view point from $q_{(1)}$ to $q_{(2)}$). *Suppose* that we follow the original "next" step in Section 4.1 which is to find the point in Q nearest to point b as the fourth point in the relative-distance representation. Similarly, due to the property that

Notation	Description
$\mathcal{P}$	A database
n	The size of a database
Q	The query point cloud
P	A point cloud in the database
Θ	A rigid transformation
$T_\Theta(p)$	The transformed point of point p wrt Θ
$T_\Theta(P)$	The transformed point cloud of P wrt Θ
$corr(q, P)$	The correspondence point of point q on P
$\|q, p\|$	The Euclidean distance between point q and point p
$dist(Q, P)$	The distance between Q and P in different coordinate systems
$rd(p_{(1)}\|p_{(2)}, p_{(3)}, p_{(4)})$	The relative-distance representation of point $p_{(1)}$ wrt $p_{(2)}, p_{(3)}$ and $p_{(4)}$
$ball(p, r)$	The r-sized ball of p
$ball\text{-}NN(p, r\|P)$	The nearest neighbor of the r-sized ball of p in P
$donut(p, r, \mathbf{n})$	The r-sized donut of p with its normal $\mathbf{n}$
$donut\text{-}NN(p, r, \mathbf{n}\|P)$	The nearest neighbor of the r-sized donut of p with its normal $\mathbf{n}$ in P
$sbz(p, [r_1, r_2])$	The sphere boundary zone of p with interval $[r_1, r_2]$
$dbz(D, [r_1, r_2])$	The donut boundary zone of D with interval $[r_1, r_2]$

Table 1: Commonly Used Notations

the distance from each query point to its correspondence point can be bounded (by Lemma 4.1), instead of following the original step *exactly*, we need to find some points in Q near to b as candidates of the fourth point $q_{(4)}$ in the relative-distance representation of $q_{(1)}$. Specifically, these points could be found in a space represented by a sphere centered at b. The following lemma shows the definition of this sphere and we could find $S_{(4)}$ containing these points.

LEMMA B.4. *Consider a query point cloud Q and a database point cloud P. Let $p_{(2)}, p_{(3)}$ and $p_{(4)}$ be the second, third, fourth owners of the relative-distance representation of point $p_{(1)}$ in P, respectively. Let $q_{(1)}, q_{(2)}$ and $q_{(3)}$ be the points in Q whose correspondence point on P are $p_{(1)}, p_{(2)}$ and $p_{(3)}$, respectively. Let m be the mid-point between $q_{(1)}$ and $q_{(2)}$, $r' = \frac{\sqrt{3}}{2}\|q_{(1)}, q_{(2)}\|$, and $\mathbf{n}$ be the vector from $q_{(2)}$ to $q_{(1)}$. Let $D = donut(m, r', \mathbf{n})$. Let a be a point on D that is nearest to $q_{(3)}$. Let b be the point at the position nearest to a in the anti-clockwise direction from a on D in the view point from $q_{(1)}$ to $q_{(2)}$ (such that $q_{(1)}, q_{(2)}, a$ and b form a regular tetrahedron). Let q' be the nearest neighbor of b in Q. Let $S_{(4)}$ be the set of all points from Q in $sbz(b, [0, \|b, q'\| + 4\triangle])$. If $dist(Q, P) \le \delta$, then there exists a point $q_{(4)}$ in $S_{(4)}$ such that $p_{(4)}$ is the correspondence point of $q_{(4)}$ on P.*

PROOF. Since $dist(Q, P) \le \delta$, by Lemma 4.1, $q_{(4)}$ also exists in Q. Applying the similar idea in the proof of Lemma B.3, we show $\|b, q_{(4)}\| \le \|b, q\| + 4\triangle$. If $\|b, q_{(4)}\| > \|b, q\| + 4\triangle$, then there exists a point in P which has smaller distance to point b than $p_{(4)}$, which contradicts that $p_{(4)}$ is the nearest neighbor of b. □

Based on the above lemma, given $q_{(1)}, q_{(2)}$ and $q_{(3)}$ (whose correspondence points on P are $p_{(1)}, p_{(2)}$ and $p_{(3)}$, respectively), we can find a set $S_{(4)}$ of *candidate* points in Q for $q_{(4)}$ inside region $sbz(b, [0, \|b, q'\| + 4\triangle])$, such that $S_{(4)}$ must contain $q_{(4)}$ which has its correspondence point on P as $p_{(4)}$, where $p_{(4)}$ is the fourth owner of the relative-distance representation of $p_{(1)}$ and can be listed out.

B.3 Extended Details of Rotation and Translation Invariant Property of Candidate Set Generation

In this section, we give the following lemma to show that the output candidate set generated by the steps of constructing the candidate set of relative-distance representations introduced in Section 4.2.4 has the translation-invariant and rotation-invariant properties.

LEMMA B.5. *Consider a query point cloud Q. Let $q_{(1)}$ be a point in Q. Let $\Theta = (R, t)$ be a transformation consisting of a rotation matrix R and a translation vector t. Consider another query point cloud Q' such that $Q' = T_\Theta(Q)$. Let $q'_{(1)}$ be a point in Q'. Let $C_{q_{(1)}}$ $(C'_{q_{(1)}})$ be the output of the steps to find the set of candidate relative-distance representations in Q (Q') with the starting point $q_{(1)}$ $(q'_{(1)})$. If $q'_{(1)} = T_\Theta(q_{(1)})$, then $C_{q_{(1)}} = C'_{q_{(1)}}$.*

PROOF SKETCH. We need to show (a) $\forall R \in C_{q_{(1)}}$, $\exists R' \in C'_{q_{(1)}}$ such that $R = R'$ and (b) the other direction of (a). For (a), consider $q'_{(i)} = T_\Theta(q_{(i)})$ for all $i \in [1, 4]$ where $q_{(i)}$ $(q'_{(i)})$ are the owners of R (R'). Then, we need to show (1) $R = R'$ and (2) $R' \in C'_{q_{(1)}}$. (1) obviously holds for a rigid transformation. (2) can be proved by showing that the 3 candidate sets in Q' with $q'_{(1)}$ contains the same points as the 3 candidate sets in Q with $q_{(1)}$. (b) can be proved by swapping $C'_{q_{(1)}}$ with $C_{q_{(1)}}$ and replacing Θ with Θ^{-1}. □

The full proof can be found in Section C.5.

B.4 Extended Details of a Heuristic Acceleration Strategy

Although the two steps of our C_2O query phase introduced in Section 4.3.2 are efficient (using index I_{DB}), we want to speed up our process with a strategy called "<u>R</u>elevancy <u>F</u>iltering" (RF).

The major idea of the RF strategy is given as follows. Note that after we choose *only one* point $q_{(1)}$ from Q in Step 1, we obtain the 2-tuple candidate set C of $q_{(1)}$ in Step 2b where C contains a number of 2-tuples each in the form of (R_Q, R_P). We could use the RF strategy to prune some of the 2-tuples in C with the following two steps to be introduced.

The first step in the RF strategy is performed just after Step 1 (and just before Step 2). Specifically, we generate a set $\mathcal{H}$ of h additional points in Q, namely $q'_{(1),1}, q'_{(1),2}, \ldots, q'_{(1),h}$, such that these h additional points are the h nearest points of $q_{(1)}$ in Q. For each point in $\mathcal{H}$, says $q'_{(1),j}$ where $j \in [1, h]$, we could also obtain a 2-tuple candidate set C'_j of $q'_{(1),j}$ (instead of $q_{(1)}$) which has the same procedure as Step 2b.

The second step in the RF strategy is performed just after Step 2b. Before we describe this second step, we first introduce a concept of "closeness" and a concept of "relevancy". Given two points $p_{(1)}$ and $p'_{(1)}$ in P and two points $q_{(1)}$ and $q'_{(1)}$ in Q, we say that pair $(p_{(1)}, p'_{(1)})$ is $\triangle$-*close* to pair $(q_{(1)}, q'_{(1)})$ if the following condition holds.

$$\|q_{(1)}, q'_{(1)}\| - 2\triangle \leq \|p_{(1)}, p'_{(1)}\| \leq \|q_{(1)}, q'_{(1)}\| + 2\triangle \tag{5}$$

In other words, when $\triangle$ is small, the distance between $p_{(1)}$ and $p'_{(1)}$ is "roughly" equal to the distance between $q_{(1)}$ and $q'_{(1)}$. If the distance between $q_{(1)}$ and $q'_{(1)}$ is small, the distance between $p_{(1)}$ and $p'_{(1)}$ is small. This $\triangle$-*closeness* relationship is the key idea for our second step which is to prune some 2-tuples in the candidate set C. Consider a 2-tuple (R_Q, R_P) in C. When $\triangle$ is small and the distance between $q_{(1)}$ and $q'_{(1)}$ is small, if pair $(p_{(1)}, p'_{(1)})$ is not $\triangle$-close to pair $(q_{(1)}, q'_{(1)})$, we know that the distance between $p_{(1)}$ and $p'_{(1)}$ is large. We could prune this 2-tuple since we expect that the distance between two query points (i.e., $q_{(1)}$ and $q'_{(1)}$) is "roughly" equal to the distance between two "matched" database points (i.e., $p_{(1)}$ and $p'_{(1)}$).

Given a 2-tuple (R_Q, R_P) in the 2-tuple candidate set C of a point $q_{(1)}$ in Q and a 2-tuple (R'_Q, R'_P) in the 2-tuple candidate set of another point $q'_{(1)}$ in Q, we say that R_P is *relevant* to R'_P wrt $(q_{(1)}, q'_{(1)})$ if (1) the ID of R_P is equal to the ID of R'_P and (2) for the first owner of R_P, namely $p_{(1)}$, and the first owner of R'_P, namely $p'_{(1)}$, pair $(p_{(1)}, p'_{(1)})$ is $\triangle$-close to pair $(q_{(1)}, q'_{(1)})$. In other words, we know that (1) the two relative-distance representations (i.e., R_P and R'_P) are in the same database point cloud and (2) the distance between the first owner of R_P and the first owner of R'_P is small if the distance between $q_{(1)}$ and $q'_{(1)}$ is small (and $\triangle$ is small).

In the above definition, we define the relevancy of a representation to another representation. Next, we overload the concept of relevancy to define the relevancy of a representation to a 2-tuple candidate set. Given (1) a 2-tuple (R_Q, R_P) in the 2-tuple candidate set C of a point $q_{(1)}$ in Q and (2) the 2-tuple candidate set C' of another point $q'_{(1)}$ in Q, we say that R_P is *relevant* to C' wrt $(q_{(1)}, q'_{(1)})$ if there exists a 2-tuple (R'_Q, R'_P) in C' such that R_P is *relevant* to R'_P wrt $(q_{(1)}, q'_{(1)})$.

With the concept of "closeness" and the concept of "relevancy", we are ready to describe this second step. This second step is to remove each 2-tuple in the form of (R_Q, R_P) from C if this 2-tuple does *not* satisfy the *complete relevancy* condition. Given (R_Q, R_P) in the candidate set C (of $q_{(1)}$), (R_Q, R_P) is said to satisfy the *complete relevancy* condition if for each candidate set C'_j (of point $q'_{(1),j}$) where $j \in [1, h]$, R_P is relevant to C'_j wrt $(q_{(1)}, q'_{(1),j})$. The reason is given as follows. Suppose that (R_Q, R_P) does not satisfy the complete relevancy condition. As long as we can find one point $q'_{(1),j}$ in $\mathcal{H}$ such that R_P is not relevant to the candidate set C'_j of $q'_{(1),j}$ wrt $(q_{(1)}, q'_{(1),j})$, for each 2-tuple $(R'_{Q,j}, R'_{P,j})$ in C'_j, R_P is not relevant to $R'_{P,j}$ wrt $(q_{(1)}, q'_{(1),j})$, and thus, we cannot obtain the "$\triangle$-closeness" relationship between $(p_{(1)}, p'_{(1),j})$ and $(q_{(1)}, q'_{(1),j})$ where $p_{(1)}$ ($p'_{(1),j}$) is the first owner of R_P ($R'_{P,j}$). It is worth mentioning that for the database point cloud P with the same ID as R_P, if $dist(Q, P) \leq \delta$, then for each $j \in [1, h]$, there exists a 2-tuple $(R'_{Q,j}, R'_{P,j})$ in C'_j such that (1) the ID of $R'_{P,j}$ is also equal to the ID of P and (2) we can obtain the "$\triangle$-closeness" relationship between $(p_{(1)}, p'_{(1),j})$ and $(q_{(1)}, q'_{(1),j})$ where $p_{(1)}$ ($p'_{(1),j}$) is the first owner of R_P ($R'_{P,j}$). Therefore, we know that "$dist(Q, P) \leq \delta$" does not hold for P, and thus, (R_Q, R_P) can be pruned.

In the following, we present a lemma to show the correctness of using the RF strategy. Specifically, let C_{RF} be the resulting candidate set of the RF strategy (i.e., C_{RF} contains all the 2-tuples in C that are not pruned). For a database point cloud P, if $dist(Q, P) \leq \delta$, C_{RF} will still contain a tuple, says (R_Q, R_P), such that each owner of R_P is the correspondence point of an owner of R_Q on P.

LEMMA B.6. *Consider a query point cloud Q and a database point cloud P. Let $q_{(1)}$ be a point in Q whose correspondence point on P is $p_{(1)}$. Let $p_{(2)}, p_{(3)}$ and $p_{(4)}$ be the second, third and fourth owners of the relative-distance representation of $p_{(1)}$, respectively. Let C_{RF} be the resulting candidate set after performing the steps of the RF strategy with the starting point $q_{(1)}$. If $dist(Q, P) \leq \delta$, then there exists a 2-tuple (R_Q, R_P) in C_{RF}, such that $R_P = rd(p_{(1)}|p_{(2)}, p_{(3)}, p_{(4)})$ and $p_{(i)}$ is the correspondence point of $q_{(i)}$ on P for $i \in [2, 4]$, where $q_{(2)}, q_{(3)}$ and $q_{(4)}$ are the second, third and fourth owners of R_Q, respectively.*

PROOF. Let C be the 2-tuple candidate set before we perform the second step of the RF strategy (i.e., before we prune some 2-tuples with the RF strategy). By the proof of Theorem 4.1 (introduced in Section C.3), we know that there exists a 2-tuple (R_Q, R_P) in C, such that $R_P = rd(p_{(1)}|p_{(2)}, p_{(3)}, p_{(4)})$ and $p_{(i)}$ is the correspondence point of $q_{(i)}$ on P for $i \in [2, 4]$, where $q_{(2)}, q_{(3)}$ and $q_{(4)}$ are the second, third and fourth owners of R_Q, respectively. Now, it is only left to show that (R_Q, R_P) will not be pruned in the RF strategy. That is, (R_Q, R_P) satisfies the *complete relevancy* condition.

Consider an arbitrary point in $\mathcal{H}$, says $q'_{(1),j}$, which is used to obtain the 2-tuple candidate set C'_j (note that we do not perform any pruning on C'_j). Since $q'_{(1),j}$ is an arbitrary point in $\mathcal{H}$, we then just need to show that R_P is relevant to C'_j wrt $(q_{(1)}, q'_{(1),j})$. Let $p'_{(1),j}$ be the correspondence point of $q'_{(1),j}$ on P. Let $p'_{(2),j}, p'_{(3),j}$ and $p'_{(4),j}$ be the second, third and fourth owners of the relative-distance representation of $p'_{(1),j}$, respectively. Since $dist(Q, P) \leq \delta$, identically, we know that there also exists a 2-tuple $(R'_{Q,j}, R'_{P,j})$ in C'_j, such that $R'_{P,j} = rd(p'_{(1),j}|p'_{(2),j}, p'_{(3),j}, p'_{(4),j})$ and $p'_{(i),j}$ is

the correspondence point of $q'_{(i),j}$ on P for $i \in [2,4]$, where $q'_{(2),j}$, $q'_{(3),j}$ and $q'_{(4),j}$ are the second, third and fourth owners of $R'_{Q,j}$, respectively. According to the definition of the relevancy of R_P to C'_j wrt $(q_{(1)}, q'_{(1),j})$, we can complete the proof by showing that R_P is relevant to $R'_{P,j}$ wrt $(q_{(1)}, q'_{(1),j})$.

The first condition is that R_P and $R'_{P,j}$ have the same ID, which is obvious since they both equal to the ID of P. The second condition is that pair $(p_{(1)}, p'_{(1)})$ is $\triangle$-close to pair $(q_{(1)}, q'_{(1)})$ (i.e., Equation 5 is satisfied). By Claim C.1 (introduced in Section C.2), since $p_{(1)}$ ($p'_{(1)}$) is the correspondence point of $q_{(1)}$ ($q'_{(1)}$) on P, Equation 5 is satisfied.　　□

C REMAINING PROOF

C.1 Proof of Lemma 4.1

PROOF. Applying Equation 3 where $Q' = T_{\Theta_o}(Q)$, we have $dist(Q, P) = [\frac{1}{|Q|}\sum_{q \in Q'}\|q', corr(q', P)\|^2]^{1/2} \le \delta$, and it is trivially derived that $\sum_{q \in Q'}\|q', corr(q', P)\|^2 \le \delta^2|Q|$. Therefore,

$$\|q', p\| = (\|q', p\|^2)^{1/2}$$
$$\le [\sum_{q \in Q'}\|q', corr(q', P)\|^2]^{1/2}$$
$$\le (\delta^2|Q|)^{1/2} = \delta|Q|^{1/2}$$

□

C.2 Proof of Lemma 4.2

PROOF. According to Lemma 4.1, since $dist(Q, P) \le \delta$, there exists $q_{(i)} \in Q$ for all $1 \le i \le 4$, such that $\|q_{(i)}, p_{(i)}\| \le \triangle$. By Lemma B.2, $S_{(2)}$ must contain $q_{(2)}$. By Lemma B.3, $S_{(3)}$ must contain $q_{(3)}$. By Lemma B.4, $S_{(4)}$ must contain $q_{(4)}$. Therefore, the candidate relative-distance representation $rd(q_{(1)}|q_{(2)}, q_{(3)}, q_{(4)})$ will be included in the result set $C_{q_{(1)}}$.

□

C.3 Proof of Theorem 4.1

PROOF. To show $\mathcal{R} = \mathcal{R}^*$, (that is, our algorithm returns the correct result set), we just need to show that there is neither false positive (FP) nor false negative (FN) in our result. Firstly, it is obvious to see that our results do not contain any false positive, because in Step 2c, we only insert the database point clouds within the δ distance threshold of query Q into the result set. Next, to show there is no FN, we show that for any database point cloud $P \in R^*$, $P \in \mathcal{R}$.

By Lemma 4.2, since $dist(Q, P) \le \delta$, the candidate set $C_{q_{(1)}}$ must contain a "desired" relative-distance representation $R_Q = rd(q_{(1)}|q_{(2)}, q_{(3)}, q_{(4)})$ that corresponds with an indexed relative-distance representation $R_P = rd(p_{(1)}|p_{(2)}, p_{(3)}, p_{(4)})$ in P. When we perform the window query for R_Q with query range $2\triangle$, R_P must also be one of the results by the definition of relative-distance representation (i.e., Equation 4). This is because, $\forall i \ne j \in [1,4]$, it holds that $\|q_{(i)}, q_{(j)}\| - 2\triangle \le \|p_{(i)}, p_{(j)}\| \le \|q_{(i)}, q_{(j)}\| + 2\triangle$ (by Lemma 4.1). Finally, in Step 2c, since we include R_P, the complete transformation Θ_o is guaranteed to be found for P, leading to $dist_{diff}(Q, P|\Theta_o) \le \delta$ (i.e., $dist(Q, P) \le \delta$).

□

C.4 Proof of Lemma B.2

PROOF. Firstly, we have the following claim, which can be easily derived from Lemma 4.1 and will be useful in our proof.

CLAIM C.1. *Consider a query point cloud Q and a database point cloud P. Let q and q' be two points in Q whose correspondence point in P are respectively p and p'. If $dist(Q, P) \le \delta$, then we have*

$$\|p, p'\| - 2\triangle \le \|q, q'\| \le \|p, p'\| + 2\triangle$$

$$\|q, q'\| - 2\triangle \le \|p, p'\| \le \|q, q'\| + 2\triangle$$

Also, according to Lemma 4.1, since $dist(Q, P) \le \delta$, there exists $q_{(2)} \in Q$, such that $\|q_{(1)}, p_{(1)}\| \le \triangle$ and $\|q_{(2)}, p_{(2)}\| \le \triangle$. Now, we show that $q_{(2)}$ is in $S_{(2)}$, which is the set of all points from Q in $sbz(q_{(1)}, [r - 2\triangle, \|q_{(1)}, q'\| + 4\triangle])$ where $q' = ball\text{-}NN(q_{(1)}, r + 2\triangle|Q)$. By definition, we need to show that $r - 2\triangle \le \|q_{(1)}, q_{(2)}\| \le \|q_{(1)}, q'\| + 4\triangle$.

Since $q' = ball\text{-}NN(q_{(1)}, r + 2\triangle|Q)$, we have $\|q_{(1)}, q'\| \ge r + 2\triangle \ge r - 2\triangle$. Thus, we show that none of the following cases is possible: $\|q_{(1)}, q_{(2)}\| < r - 2\triangle$ or $\|q_{(1)}, q_{(2)}\| > \|q_{(1)}, q'\| + 4\triangle$.

(1) Since $p_{(2)} = ball\text{-}NN(p_{(1)}, r|P)$, we have $\|p_{(1)}, p_{(2)}\| \ge r$. Therefore, by Claim C.1, $\|q_{(1)}, q_{(2)}\| \ge \|p_{(1)}, p_{(2)}\| - 2\triangle \ge r - 2\triangle$, indicating that the first inequality cannot hold.

(2) Assuming the third inequality holds, since $\|q_{(1)}, q_{(2)}\| \le \|p_{(1)}, p_{(2)}\| + 2\triangle$ (by Claim C.1), we have $\|p_{(1)}, p_{(2)}\| > \|q_{(1)}, q'\| + 2\triangle$. Let p' be the correspondence point to q' in P. Again by Claim C.1, we have $\|p_{(1)}, p'\| \in [\|q_{(1)}, q'\| - 2\triangle, \|q_{(1)}, q'\| + 2\triangle]$, and thus we must have $\|p_{(1)}, p'\| < \|p_{(1)}, p_{(2)}\|$. Moreover, since $\|q_{(1)}, q'\| \ge r + 2\triangle$, the lower bound of $\|p_{(1)}, p'\|$ is r, indicating that point p' is closer to the r-sized ball centered at $p_{(1)}$. This leads to a contradiction with $p_{(2)} = ball\text{-}NN(p_{(1)}, r|P)$.

Therefore, we have $q_{(2)} \in sbz(q_{(1)}, [r - 2\triangle, \|q_{(1)}, q'\| + 4\triangle])$. Since $q_{(2)}$ is a point of Q, by definition, we have $q_{(2)} \in S_{(2)}$.

□

C.5 Proof of Lemma B.5

PROOF. We show that $C_{q_{(1)}} = C'_{q_{(1)}}$ by the following two claims: (1) for each $rd(q_{(1)}|q_{(2)}, q_{(3)}, q_{(4)}) \in C_{q_{(1)}}$, there exists a relative-distance representation $rd(q'_{(1)}|q'_{(2)}, q'_{(3)}, q'_{(4)}) \in C'_{q_{(1)}}$ such that $rd(q_{(1)}|q_{(2)}, q_{(3)}, q_{(4)}) = rd(q'_{(1)}|q'_{(2)}, q'_{(3)}, q'_{(4)})$ and (2) for each $rd(q'_{(1)}|q'_{(2)}, q'_{(3)}, q'_{(4)}) \in C'_{q_{(1)}}$, there exists a relative-distance representation $rd(q_{(1)}|q_{(2)}, q_{(3)}, q_{(4)}) \in C_{q_{(1)}}$ such that $rd(q_{(1)}|q_{(2)}, q_{(3)}, q_{(4)}) = rd(q'_{(1)}|q'_{(2)}, q'_{(3)}, q'_{(4)})$.

For the first claim, consider that $q'_{(2)} = T_\Theta(q_{(2)})$, $q'_{(3)} = T_\Theta(q_{(3)})$ and $q'_{(4)} = T_\Theta(q_{(4)})$. Next, we need to show that $rd(q_{(1)}|q_{(2)}, q_{(3)}, q_{(4)}) = rd(q'_{(1)}|q'_{(2)}, q'_{(3)}, q'_{(4)})$ and $rd(q'_{(1)}|q'_{(2)}, q'_{(3)}, q'_{(4)}) \in C'_{q_{(1)}}$.

Firstly, since for each $i \in [1,4]$, $q'_{(i)}$ is the transformed point of $q_{(i)}$ by the same transformation Θ, it is obvious that the distance between each pair-wise distance among the four points remains unchanged. Therefore, by the definition of relative-distance representation (i.e., Equation 4), it is easy to get $rd(q_{(1)}|q_{(2)}, q_{(3)}, q_{(4)}) = rd(q'_{(1)}|q'_{(2)}, q'_{(3)}, q'_{(4)})$.

Secondly, we perform the steps to find the set of candidate relative-distance representations with the same Q, r and $\triangle$ starting from $q_{(1)}$ and $q'_{(1)}$, respectively, as two *instances* denoted by $\mathcal{I}$ and $\mathcal{I}'$, respectively. We continue our proof by showing that we obtain the sets of same points in $S_{(2)}$, $S_{(3)}$ and $S_{(4)}$ for $\mathcal{I}$ and $\mathcal{I}'$, and in the following we say that $q \in Q$ and $q' \in Q'$ are the same points if $q' = T_\Theta(q)$.

(1) Let q' (q'') be the *ball-NN* operation result we obtain (i.e., $ball\text{-}NN(q_{(1)}, r + 2\triangle | Q)$) for $\mathcal{I}$ ($\mathcal{I}'$). Since Q' is obtained by transforming every point in Q with the same transformation Θ, we know that the distance between every other point to $q_{(1)}$ remains unchanged. Therefore, the *ball-NN* operation result also remains unchanged (i.e., $q'' = T_\Theta(q')$). And then, we can obtain the same set of points inside $sbz(q_{(1)}, [r - 2\triangle, \|q_{(1)}, q'\| + 4\triangle])$ for $\mathcal{I}$ and $\mathcal{I}'$. Further, let $S'_{(2)}$ be the set we obtain in Step (i) for $\mathcal{I}'$. By the above result, $S'_{(2)}$ must contain $q'_{(2)}$ which equals to $T_\Theta(q_{(2)})$.

(2) In Step (i)(1), we focus on the case of $q_{(2)}$ ($q'_{(2)}$) for $\mathcal{I}$ ($\mathcal{I}'$). Let m', $\mathbf{n}'$, r'' be the result of the mid-point between $q'_{(1)}$ and $q'_{(2)}$, the vector from $q'_{(2)}$ to $q'_{(1)}$ and $\frac{\sqrt{3}}{2}\|q'_{(1)}, q'_{(2)}\|$, respectively, for $\mathcal{I}'$. Then, it is also obvious that $m' = T_\Theta(m)$, $\mathbf{n}' = T_\Theta(\mathbf{n})$ and $r'' = r'$. As such, we also obtain a donut D' for $\mathcal{I}'$ which contains exactly the same points as D. Again, due to rigid transformation, the distance between every point in Q to D remains unchanged. Thus, we get the same resultant point for the *donut-NN* operation and thus can obtain the same set of points inside $dbz(D, [0, dist(q', D) + 4\triangle])$ for $\mathcal{I}$ and $\mathcal{I}'$. Let $S'_{(3)}$ be the set we obtain in Step (i)(1) for $\mathcal{I}'$. By the above result, $S'_{(3)}$ must contain $q'_{(3)}$ which equals to $T_\Theta(q_{(3)})$.

(3) In Step (i)(1)(I), we focus on the case of $q_{(3)}$ ($q'_{(3)}$) for $\mathcal{I}$ ($\mathcal{I}'$). Let a' and b' be the two virtual points for $\mathcal{I}'$. Since again all the points remain their distance to D, then we have $a' = T_\Theta(a)$ and $b' = T_\Theta(b)$. Thus, we can obtain the same set of points inside $sbz(b, [0 \|b, q''\| + 4\triangle])$ for $\mathcal{I}$ and $\mathcal{I}'$. Let $S'_{(4)}$ be the set we obtain in Step (i)(1)(I) for $\mathcal{I}'$. By the above result, $S'_{(4)}$ must contain $q'_{(4)}$ which equals to $T_\Theta(q_{(4)})$. Finally, we will obtain a relative-distance representation $R = rd(q'_{(1)}|q'_{(2)}, q'_{(3)}, q'_{(4)})$ and include it in the result set $C'_{q'_{(1)}}$.

Till now, we have proved the first claim. Consider the reverse transformation of Θ (i.e., Θ^{-1}). Then, we have $Q = T_{\Theta^{-1}}(Q')$ and $q_{(1)} = T_{\Theta^{-1}}(q'_{(1)})$. Thus, we can directly prove the second claim by swapping Q with Q', swapping $q_{(1)}$ with $q'_{(1)}$ and substituting Θ with Θ^{-1}.

$\square$

D ADDITIONAL EXPERIMENTAL RESULTS

We show our additional experimental results in the following parts. In Section D.1, we show the detailed results of studying the design of our C_2O algorithm. In Section D.2, we show the additional results for dataset *Object*. In Section D.3, we show the all the experimental results for dataset *Indoor*.
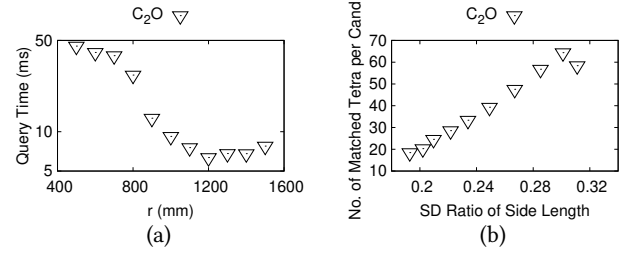

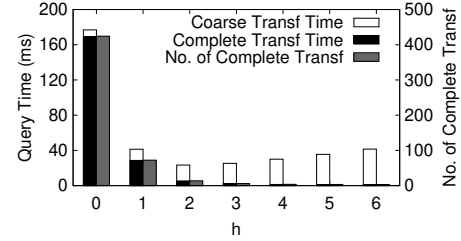**Figure 9: Effect of Indexed Tetrahedra Size and Regularity of C_2O for Dataset *Object***
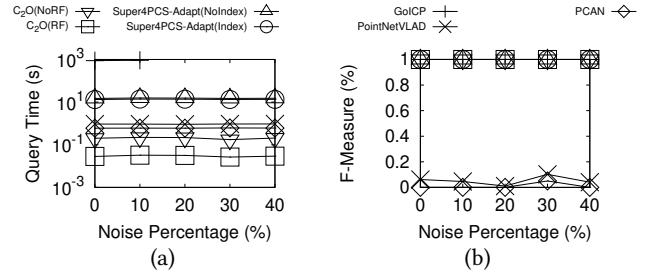

Figure 10: Effect of the *RF* Strategy

Figure 11: Effect of Noise Percentage for Dataset *Object*

D.1 Detailed Results of Studying the Design of Our C_2O Algorithm

Study of Parameter in our C_2O framework: We studied the major parameter in our C_2O framework, namely r (i.e, the side length of a tetrahedron). For the default setting of dataset *Object*, we build our C_2O index with varied radius r ranging from 500mm to 1,500mm. We take the average values to report experimental results.

In this experiment, after we set r to a value, we obtain an index based on a number of tetrahedra constructed in our C_2O index. Based on each index, we could issue queries described before and measure the query time. As illustrated in Figure 9(a), when r increases, the query time decreases first, reaches the minimum query time when r reaches around 1,200mm and increases after that. The reason is that smaller tetrahedra (with smaller r values) tend to trigger more (expensive) complete transformations in the database, which is consistent with existing observations [24] (since it is very likely that a small given tetrahedron is "similar" to a lot of small tetrahedra due to the *micro-view* (or too detailed view) from this
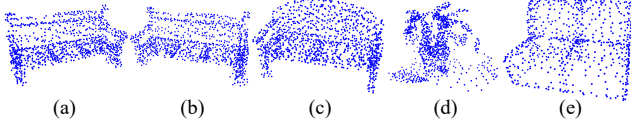
(a)　　　(b)　　　(c)　　　(d)　　　(e)
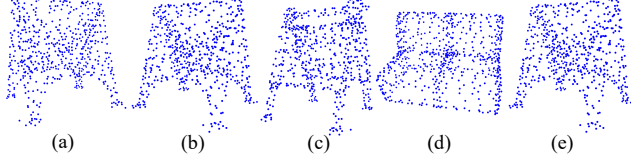
Figure 12: Case Study with Query Object as Bench

(a)　　　(b)　　　(c)　　　(d)　　　(e)

Figure 13: Case Study with Query Object as Standing Sign
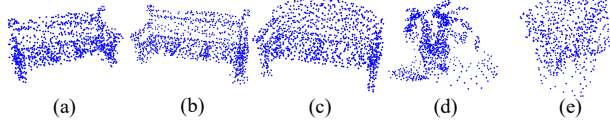

(a)　　　(b)　　　(c)　　　(d)　　　(e)

Figure 14: Case Study with the Query Object of a Bench with Noise

given tetrahedron, resulting in a non-distinguishable tetrahedron). However, when r is very large, the cost of spatial operations (e.g. queries finding *ball-NN*) becomes higher and thus, the query time is larger. According to this, we set r = 1,200mm leading to the best-performing C_2O for the *Object* databases, and for dataset *Indoor*, we set r = 350mm following the similar trends in our experiments.

Study of Regularity of Tetrahedron: Next, we study why the regularity of a tetrahedron, the major principle used in our C_2O framework, is used. We also used the same experimental setup as the above experiment to build our C_2O index. In this experiment, the regularity of a tetrahedron could be described by the SD (S̲tandard D̲eviation) ratio of side length which is defined to be the SD over the 6 side lengths divided by the average side length. A more regular tetrahedron tends to have similar side lengths, resulting in a smaller SD. Here, adopting the (relative) ratio (i.e., the SD divided by the average side length) instead of the absolute SD value is to study the regularity (which is relative in nature). We measure the number of database tetrahedra matched for each query tetrahedron candidate for each indexed tetrahedron.

Figure 9(b) shows that, in general, the number of database tetrahedra matched for each query tetrahedron candidate increases when the SD ratio increases. This means that less regularity (larger SD ratio) leads to more matched tetrahedra to be verified, leading to a larger query time. This could justify our strategy of using more regular tetrahedra (where the SD ratio is smaller).

Effect of Relevancy Filtering (RF) Strategy: In Section B.4, we propose the *RF* strategy to reduce the number of complete transformations by selecting h additional nearby query points for pruning. We now show how much query time this strategy improves and what value h to select by varying h from 0 (our algorithm without RF) to 6.
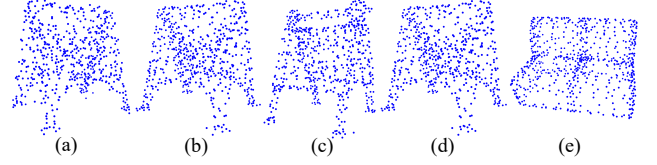

(a)　　　(b)　　　(c)　　　(d)　　　(e)

Figure 15: Case Study with the Query Object of a Standing Sign with Noise

As illustrated in Figure 10, the *RF* strategy improves the overall query time, including both the coarse transformation time and the complete transformation time, significantly. Although the coarse transformation time (white bar) increases with h (since we perform more coarse transformation operations), the complete transformation time (black bar) decreases dramatically since the number of complete transformations (grey bar) decreases by 1–2 orders of magnitudes. However, when $h > 2$, the coarse transformation time begins to dominate the total query time, causing the total query time to increase slightly. We thus fix h to be 2 in the rest of the experiments for the best performance. For the remaining experimental results, and we use $\mathbf{C_2O(RF)}$ to denote our algorithm with the RF strategy. We also include the original algorithm (denoted by $\mathbf{C_2O(NoRF)}$) to fully show the effectiveness of the RF strategy.

D.2 Additional Results on Dataset *Object*

We first show the detailed results on the effect of noise percentage on dataset *Object* in Section D.2.1, then we show the additional case studies on dataset *Object* in Section D.2.2, and finally we present the detailed results of different types of queries on dataset *Object* in Section D.2.3.

D.2.1 Effect of Noise Percentage on Dataset Object. Figure 11(a) shows that the noise percentage does not affect the query times of all algorithms. In particular, $\mathbf{C_2O(RF)}$ gives the smallest query time. Figure 11(b) shows that the F-measure of all algorithms except deep learning algorithms is 100% but that of deep learning algorithms is only around or less than 15%.

D.2.2 Additional Case Studies on Dataset Object. In this experiment, we would like to study two case studies about the results returned by our proposed algorithm and the deep learning algorithms. Figure 12 shows the first case study where Figure 12(a) shows the query object. Consider the object retrieval query where δ is set to 20% of the query object diameter. Our proposed algorithms return the exact object (as shown in Figure 12(b)) (as the most similar object) and the second similar object (as shown in Figure 12(c)). However, the deep learning algorithm **PointNetVLAD** returns two irrelevant objects as shown in Figures 12(d) and (e). We also have the second case study as shown in Figure 13 where the query object is a standing sign as shown in Figure 13(a). Similarly, the results of our proposed algorithms are shown in Figures 13(b) and (c) which "look" similar to the query object. The deep learning algorithm **PointNetVLAD** returns two objects as shown in Figures 13(d) and (e). Though the second object returned by **PointNetVLAD** is the desired output, the first object returned does not look similar to the query object.

Besides, we conducted the above case studies where the noise percentage is set to 40% and all the other parameters are the same. For the first case, even when the query object (a bench) contains intense noise, our proposed algorithm still returns not only the most similar object, which is actually the exact object without noise (as shown in Figure 14(b)), but the second similar object (as shown in Figure 14(c)) as well. The deep learning algorithm **PointNetVLAD** however returns two irrelevant objects (as shown in Figures 14(d) and (e)). Similar results are obtained for the second case where the query object is a standing sign with noise. Our algorithm returns two similar standing signs from the database (as shown in Figures 15(b) and (c)), while **PointNetVLAD** only returns one similar object (as shown in Figure 15(d)), but another output is irrelevant (as shown in Figure 15(e)). Note that the other deep learning algorithm **PCAN** gives similar inaccurate results.

D.2.3 Results of Different Types of Queries on Dataset Object. In this part, we demonstrate the comparison among all algorithms of dataset *Object* for different types of queries as described in Section 6.1.2. Specifically, the results for the second-type, third-type, fourth-type and fifth-type queries are reported in Figure 16, 17, 18 and 19, respectively.

The result we obtain for each of the other query types is similar to that the first type of queries (as shown in Figure 8 and 11). For the types of queries which contain more query objects outside the database (i.e., the second-type queries 100% of which are outside the database, and the fourth-type queries 80% of which are outside the database), we observe that all the non-deep learning algorithms use slightly more time to execute the queries (as shown in Figure 16 and 18, respectively) than the other types, but our proposed algorithms still have the shortest query times among all the non-deep learning algorithms for all the query types. Specifically, in the default setting, when the type of queries is switched from the first-type to the second-type, the query time of our $C_2O(RF)$ algorithm increases from 0.032s to 0.04s, while the query time of the fastest existing non-deep learning algorithm (i.e., **Super4PCS-Adapt(Index)**) increases from 13.9s to 22s.

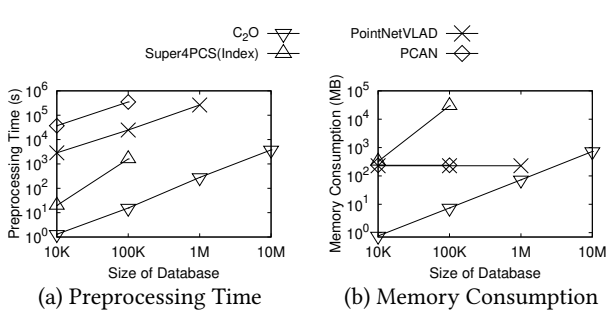## D.3 Experimental Results on Dataset *Indoor*

In this part, we report the detailed experimental results on dataset *Indoor*.

Firstly, we show the query time of our algorithm C_2O with the effect of *r* in Figure 20. We set *r* ranging from 50mm to 500mm for dataset *Indoor*. We observe the similar trend as for dataset *Object* (as shown in Figure 9(a)). Specifically, the query time first drops when *r* increases from 50mm to 350mm and then increases slightly when *r* is larger than 350mm. Therefore, we set *r* = 350mm for all the experiments on dataset *Indoor* since it leads to the smallest query time.

Next, we also show the comparison results of preprocessing time and memory consumption for all the algorithms that need preprocessing for dataset *Indoor*. The results show that, for dataset *Indoor*, our preprocessing step is significantly faster than that of the existing index-based algorithm and all the deep learning algorithms (as shown in Figure 21(a)). Moreover, as shown in Figure 21(b), the memory consumption of our algorithm C_2O is also much more efficient than that of the index-based algorithm **Super4PCS-Adapt(Index)**

which reaches about 20GB even when the size of database is 100K. Note that the memory consumption of our algorithm C_2O is only about 800MB for the largest size of database with over 10M points.

We also run queries on dataset *Indoor* with all types of queries for all the factors we study. The results are reported in Figure 22, 23, 24, 25 and 26 for the first-type, second-type, third-type, fourth-type and fifth-type queries, respectively. All the results are similar to those on dataset *Object*.
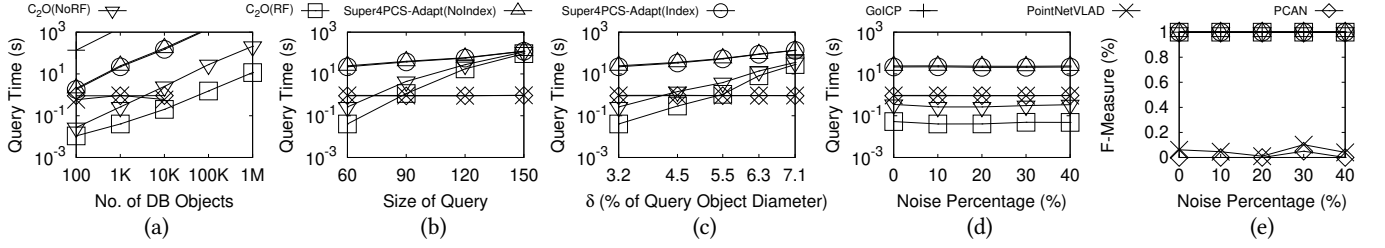
Figure 16: Effect of Size of Database, Size of Query, δ and Noise Percentage for Dataset *Object* with the Second-type Queries
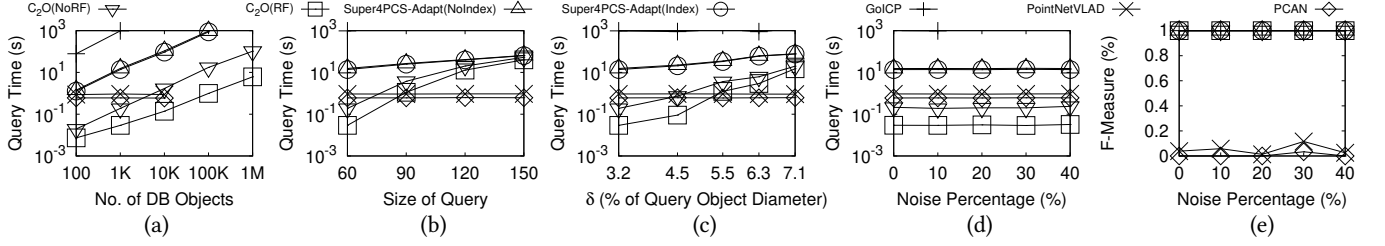
Figure 17: Effect of Size of Database, Size of Query, δ and Noise Percentage for Dataset *Object* with the Third-type Queries
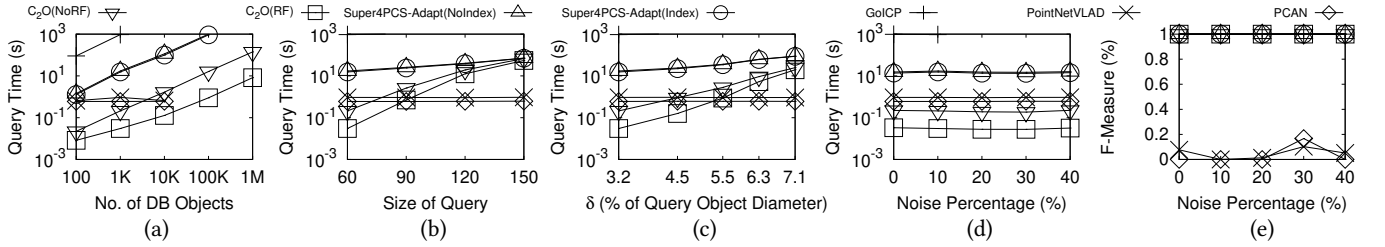
Figure 18: Effect of Size of Database, Size of Query, δ and Noise Percentage for Dataset *Object* with the Fourth-type Queries
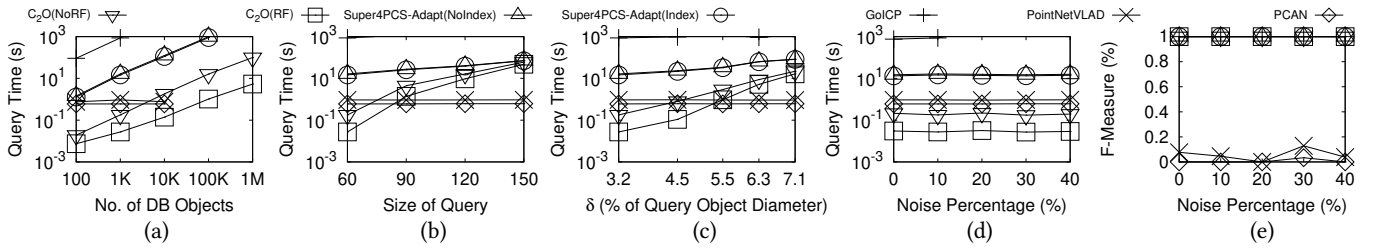
Figure 19: Effect of Size of Database, Size of Query, δ and Noise Percentage for Dataset *Object* with the Fifth-type Queries

(a) Preprocessing Time　　(b) Memory Consumption

Figure 21: Preprocessing Time and Memory Consumption for Dataset *Indoor*

Figure 20: Effect of Indexed Tetrahedra Size for Dataset *Indoor*
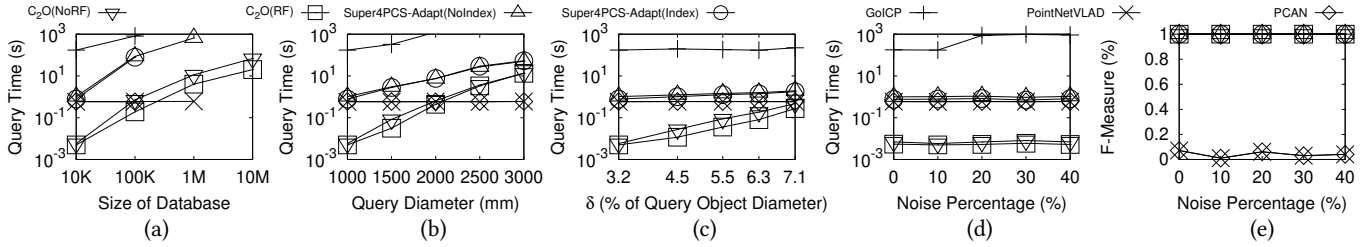
Figure 22: Effect of Size of Database, Size of Query, δ and Noise Percentage for Dataset *Indoor* with the First-type Queries
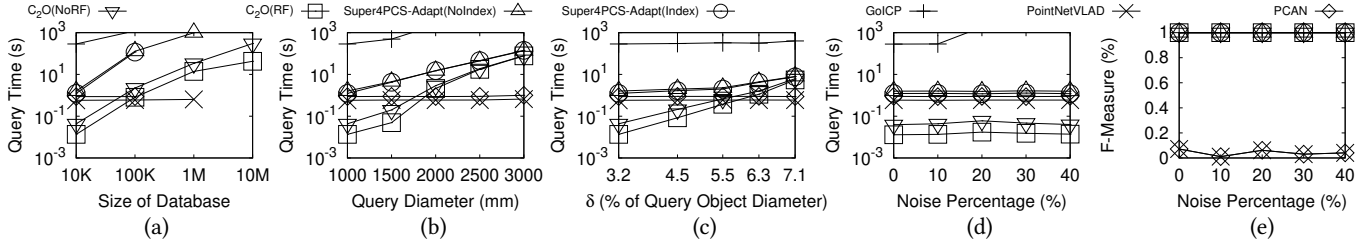
Figure 23: Effect of Size of Database, Size of Query, δ and Noise Percentage for Dataset *Indoor* with the Second-type Queries
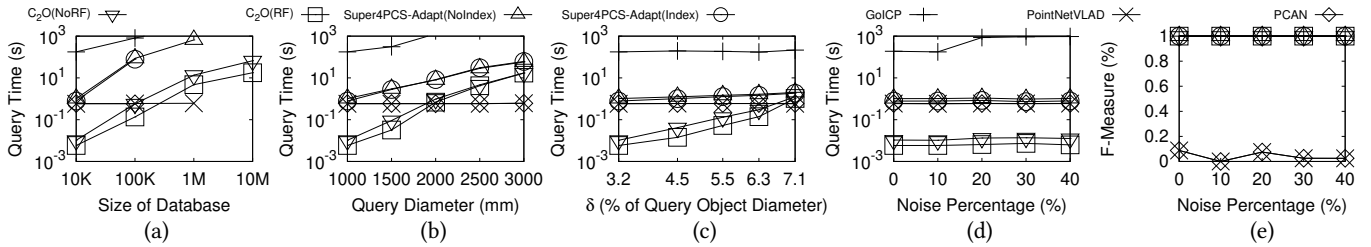
Figure 24: Effect of Size of Database, Size of Query, δ and Noise Percentage for Dataset *Indoor* with the Third-type Queries
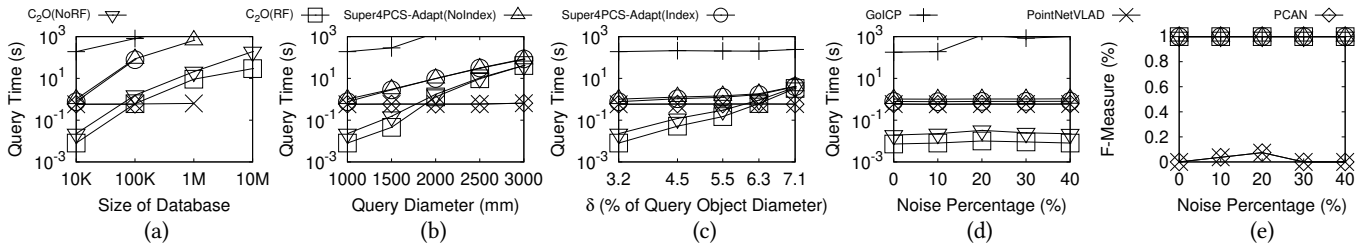
Figure 25: Effect of Size of Database, Size of Query, δ and Noise Percentage for Dataset *Indoor* with the Fourth-type Queries
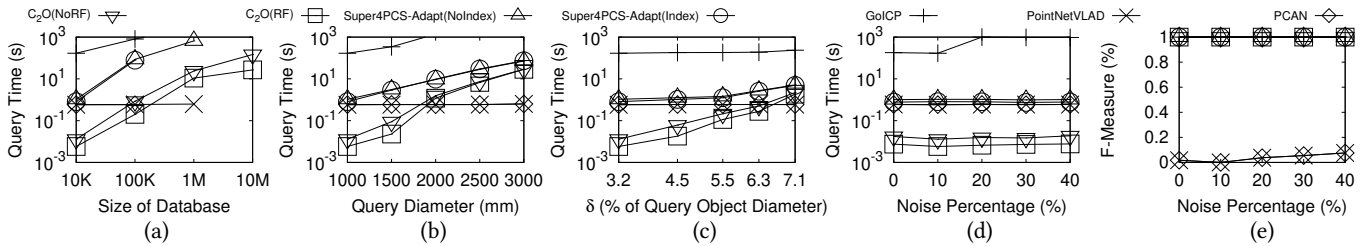
Figure 26: Effect of Size of Database, Size of Query, δ and Noise Percentage for Dataset *Indoor* with the Fifth-type Queries